Early Pleistocene depositional and environmental conditions at Dachangliang, Nihewan Basin, NE China

Ahmed H. Moghazi[1]*, Hailong Zhao[2,3]*, Chengjun Zhang[4], Elísabet A. Eythorsdottir[1,5] and Steffen Mischke[1]

[1]Institute of Earth Sciences, University of Iceland, Reykjavík, Iceland, [2]School of Archaeology and Museology, Liaoning University, Shenyang, Liaoning, China, [3]College of History and Culture, Hebei Normal University, Shijiazhuang, Hebei, China, [4]College of Earth Sciences and Key Laboratory of Mineral Resources in Western China, Lanzhou University, Lanzhou, Gansu, China, [5]Institute of Life and Environmental Sciences, University of Iceland, Reykjavík, Iceland

The Pleistocene sediments of Nihewan Basin in NE China are intensively studied since ca. 100 years because of its rich mammalian fossil record and abundant stone-artifact-bearing layers. To better understand the mechanisms underlying past climate and environmental changes in the basin, three sediment sections at the Dachangliang location were investigated using a multi-proxy toolbox of sedimentological, magnetic susceptibility (MS) and micropalaeontological analyses. The exposed sediments are lithologically mostly relatively homogeneous, with grain sizes in a relatively small range. However, variations in colour, bedding structures, concentrations of magnetic minerals and the ostracod assemblage were used to correlate the three sections to form the synthetic NH-T section of 86.2-m total length. The sediments mainly represent varicoloured silt of probably reworked loess deposits, partially interbedded with fine sand layers and minor contributions of clay particles. These sediments are interpreted to have accumulated in wetlands alternating with deposition on an alluvial plain, and with a lacustrine setting which probably existed from time to time. These different depositional settings are expressed in the three dominant fine to coarse silt-sized components and the ostracod-assemblage changes (mostly *Limnocythere flexa*, *Ilyocypris* spp. and *Leucocythere* sp.). The recorded ostracods of laterally apparently consistent white marl beds (dominantly *Cytherissa lacustris*) were used to stratigraphically correlate these sections. The resulting NH-T section was further correlated with the three proximal artefact-bearing sections Majuangou, Banshan and Xiantai which have published magnetostratigraphic data. The correlation shows that the investigated sedimentary sequence was probably formed between ca. 1.7 and 0.9 Ma. The relatively continuous synthetic sequence NH-T represents three main wetter periods with three intervening drier intervals, possibly synchronous with interglacial (S_{23}–S_{20}, S_{15}–S_{13} and S_{10}–S_9) and glacial (L_{20}–L_{18}, L_{17}–L_{16} and L_{13}–L_{11}) periods which were previously inferred from the palaeoclimatic records of the Chinese Loess Plateau (CLP) in the SW of the Nihewan Basin.

KEYWORDS

Quaternary, Ostracoda, Palaeoclimate, Early humans, Palaeolithic

1 Introduction

The study of the Early Pleistocene sediments in the Nihewan Basin, NE China, plays a key role in our understanding of the Quaternary natural and cultural history, and the interaction between early humans and the environment in N China. The Nihewan Basin is a late Cenozoic intermontane rift with a thick succession of lacustrine and fluvial sediments from the late Pliocene to the Late Pleistocene (Wei, 1991). The Nihewan Basin is significant in Quaternary geological research in China due to its continuous sedimentation and it is known for its fossil remains of the Pleistocene megafauna and rich source of lithic artifacts (Barbour, 1924; Teilhard de Chardin and Piveteau, 1930; Deng et al., 2008; Yang et al., 2019). As such, it has become an important location for investigating Quaternary palaeontology, palaeoenvironment, and Palaeolithic archaeology at high latitudes in E Asia, providing valuable insights into the evolution and behavior of early humans in the region following the earliest "Out of Africa" migration (Schick et al., 1991; Zhu et al., 2001; Zhu et al., 2004; Dennell, 2013). The most widely known Quaternary studies in the Nihewan Basin have focused on documenting and examining the technology of stone tools, describing megafaunal components, and using magnetostratigraphy to date lithic artifact-bearing sediment sections (Wei, 1983; Xia, 1992; Qiu, 2000; Deng and Zheng, 2005; Wang et al., 2005; Deng et al., 2006b; Wang et al., 2006; Deng et al., 2007; Deng et al., 2008; Liu et al., 2010; Ao et al., 2012; Ao et al., 2013a). The earlier inferences of Xia (1992) on the ancient lake shoreline changes in the Nihewan Basin indicated two periods of advance and three periods of retreat, forming terraces during the early and middle Pleistocene. In contrast, Li et al. (2008) suggested two longer lasting lacustrine periods with the accumulation of fluvio-lacustrine deposits in between based on their work on the exposed fluvio-lacustrine sequence at Xiaodukou (120-m thick, ca. 1.8–0.1 Ma, correlated to marine isotope stages 64 to 11) in the Nihewan Basin. Some more recent studies provided a very schematic or cursory perspective of the basin evolution. For example, Chen et al. (2015) suggested that the Nihewan Basin underwent three major stages of evolution including expansion, contraction, and extinction, as indicated by the lacustrine, deltaic, and alluvial fan deposits which formed at 2.6, 1.8, and 0.11 Ma, respectively. Furthermore, the inferred paleo-lake history of the Taiyuan and Linfen grabens in N China, includes three periods of regressions in lake level followed by the deposition of loess during the Pleistocene (Hu et al., 2005). Despite over a century of research in the basin, the published literature presents conflicting interpretations of the complex depositional history in the Nihewan Basin. In addition, detailed sedimentological and micropalaeontological analysis of long stratigraphic Early Pleistocene sediment sections in the basin are missing. Thus, our work had the aim to provide a better understanding of 1) the Early Pleistocene depositional setting at Dachangliang in the Nihewan Basin, and 2) to establish a lithological and stratigraphic correlation between the Dachangliang deposits and the neighbouring well-dated palaeolithic sites in the E margin of the Nihewan Basin. We conducted a multi-proxy study, including the analyses of grain size, sediment colour, sedimentary structures, magnetic mineral concentrations, and ostracod assemblage of the deposits. The presented data are fundamental for a better understanding of the climate and environment during the Early Pleistocene, and their significance for the early periods of hominin occupation in the region.

2 Study area

The Early Pleistocene deposits of Dachangliang are exposed at the E margin of the Nihewan Basin in Yangyuan County, Hebei Province. The basin is located at the NE margin of the Loess Plateau, in the transitional zone between the Inner Mongolia Plateau and the N China Plain (Figure 1). The basin is located in the NE part of the Shanxi Graben System, which developed in the region of Taihang Mountains and Yanshan Mountains during the Middle and Late Pliocene as a series of intermontane basins (Li et al., 1998). The Nihewan Basin is a NE–SW elongate graben structure with a floor at ca. 800–900 m above sea level, encompassing an area of about 80-km length and 15–20-km width. It is bounded by the Xiong'er Mountain to the N, the Liuleng Mountains to the S, the Fenghuang Mountains to the E and the Guancen Mountain to the SW. The basin is structurally separated by the Youfang dip-slip fault into two sub-basins: the Yangyuan sub-basin lies in the N and the Yuxian sub-basin in the S. The Nihewan deposits cover Archaean gneiss and Sinian quartzites (Xiong'er Mt.), Palaeozoic marine strata (Liuleng Mts.) and Mesozoic volcaniclastic rocks. Paleogene basalts and gravels occur occasionally within the basin in the SE of the Liuleng Mountains. Nihewan Basin accumulated a relatively continuous archive of fluvio-lacustrine sediments in a semi-deep to shallow palaeolake during the Late Pliocene to Middle Pleistocene. With tectonic development of a graben basin, reworked reddish sediments of aeolian origin were initially accumulated within the basin during the Early Pliocene. Subsequently, the basin became completely invaded by Nihewan palaeolake in the Middle-Late Pliocene (Ao et al., 2013b; Liu et al., 2018). During the Early to Middle Pleistocene, the water body began to disappear gradually and finally dried up (Xia, 1992). Afterwards, the lacustrine environment was replaced by a fluvial setting with the ancient tributaries of the Sanggan River flowing from SW to the NE through the basin (Wei, 2016). This depositional history resulted in the succession of the so-called "Nihewan Beds" (Barbour, 1924) or the Nihewan Formation (Min and Chi, 2003) that represents the type section of the Early Pleistocene in N China (Young, 1950). Today, the fluvio-lacustrine sequences are capped by wind-blown deposits from the last glaciation. Chi and Wei (2013) divided the sedimentary succession of the Nihewan Basin (approximately 700 m) into five lithostratigraphic units ranging in age from Pliocene to Holocene as follows: 1) the Pliocene Yuxian Formation, 2) the early Pleistocene Nihewan Formation, 3) the middle Pleistocene Xiaodukou Formation, 4) the late Pleistocene Xujiayao Formation, and 5) the Holocene Shibaozhuang Formation. Confusingly, the entire sedimentary fill of the basin was also termed the Nihewan Beds (Barbour, 1924) and renamed the Nihewan Formation in recent years (Deng et al., 2008).
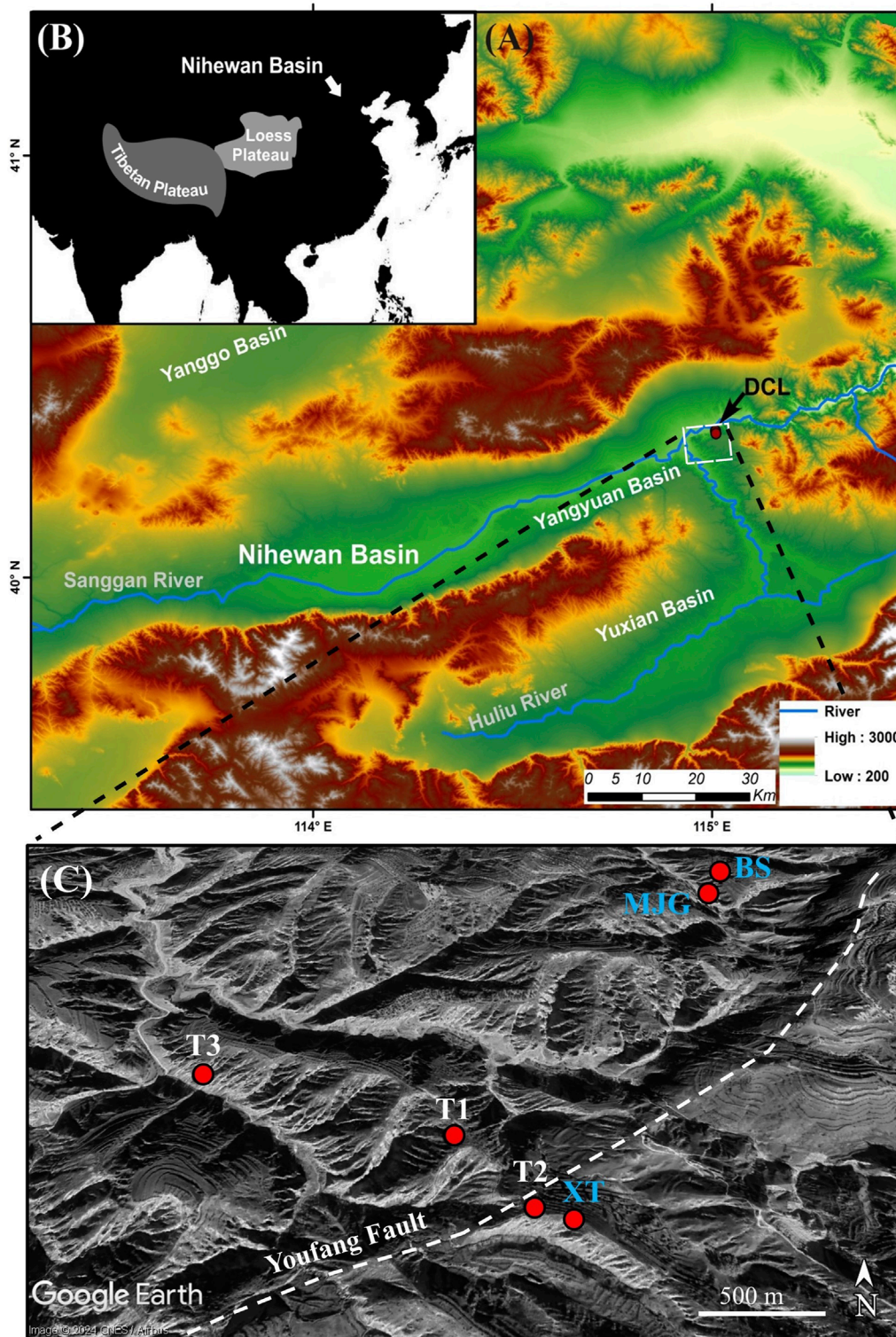
FIGURE 1
Location of the study area Dachangliang (DCL) in the Nihewan Basin **(A)** and general position in Asia **(B)**. Locations of the T1, T2 and T3 sections (white labels) and the neighbouring Paleolithic sites (Majuangou (MJG), Banshan (BS) and Xiantai (XT); blue labels; **(C)**.

2.1 Dachangliang age

Magnetostratigraphic analysis of fluvio-lacustrine sediments at Dachangliang implied that sediments accumulated from the lower Olduvai subchron to the late Brunhes chron (Deng et al., 2006b). The age of the artifact-bearing layer at Dachangliang site, discovered in August 2000, and excavated in September 2000 and also in July and August 2001, is about 1.36 Ma based

on the correlation of magnetostratigraphic, lithostratigraphic and magnetic susceptibility data with the neighbouring well-known Xiaochangliang site (Pei, 2002; Deng et al., 2006b). The latest astronomical dating shows that the estimated age of the artefact layer at the Dachangliang site is 1.48 Ma (Ao et al., 2010b), slightly older than the Xiaochangliang site. The Majuangou-III site, only ca. 1 km to the NE of Dachangliang, is the oldest well-dated site in the NE China, dating back to approximately 1.66 Ma. In contrast, the earliest evidence for the presence of hominins in China is dated to around 2.1 Ma at the Shangchen site located ca. 800 km to the SW on the S Loess Plateau (Yang et al., 2019).

2.2 Hydrology

The Nihewan Basin is fed by a number of small rivers and streams, and it is drained by the Sanggan River, its tributary, the Huliu River. The Sanggan River originates from the SW mountains (mainly Guancen Mountain) and meanders through the Datong and Yangyuan sub-basins in a NE direction. Today, the Sanggan River flows out of the basin through the Sanggan Gorge at the province of Shanxi. The Huliu River, the main tributary, drains the S Yuxian sub-basin and joins the Sanggan River in the NE part of the Nihewan Basin.

2.3 Climate

The climate in the basin is semi-arid, controlled by the winter and summer monsoon with distinct seasonal changes. Winters are cold, dry, and influenced by prevailing NW winds (winter monsoon) which originate from the cold Mongolian High. Conversely, the region is characterized by high temperatures and abundant precipitation in the summer owing to the effect of SE winds (summer monsoon) driven by low pressure over the continent and high pressure over the N Pacific (Domrös and Peng, 1988). The mean annual temperature is 7.7°C with a mean January temperature of ca. −16°C, and mean July temperature of ca. 29°C (Yangyuan County Weather Station, 1980–2019; data source: China Meteorological Data Network, http://data.cma.cn). Mean annual precipitation is 347.8 mm (1980–2019), with the majority occurring during the summer months.

2.4 Vegetation, current human impact

The regional vegetation includes temperate steppe in the interior of the basin and temperate deciduous shrubland in the mountainous regions (Mu et al., 2015). Typical grassland taxa such as *Artemisia*, Gramineae and Asteraceae dominate below 1200 m asl. However, most of the flat alluvial areas adjacent to the rivers and streams are used for cultivation, and the main crops are *Zea mays* (corn), *Sorghum bicolor* (great millet) and *Setaria italica* (foxtail millet; Li et al., 1996). Between 1200 and 1600 m asl, mixed forests of coniferous and broadleaved trees such as *Betula phatyphylla*, *Quercus*, *Carpinus* and *Pinus tabulaeformis*, and deciduous shrubs (*Ostryopsis* and *Spiraea salicifolia*) occur. Above

1600 m asl, cold-resistant coniferous forests mainly include *Larix principis-rupprechtii*, *Picea wilsonii* and *Pinus*.

3 Materials and methods

3.1 Field work

Three sediment sections were newly exposed on the SW slope of the Dachangliang ridge at 40.2199 °N and 114.6589°E (T1), 40.2190°N and 114.6598°E (T2) and 40.2212 °N and 114.6549 °E (T3), respectively (Figure 1). The tops of the T1, T2 and T3 sections were determined to be 894.04, 906.31 and 861.76 m, respectively, using a hand-held Qianxun SI (SR6) GPS receiver, a laser rangefinder and a tape. The lithology of the exposed sediments was described in detail including grain size, sedimentary bedding structures, pedogenic features (carbonate nodules, root casts, mottling, animal burrows, etc.), macroscopic fossils (mostly gastropod shells) and colour using the Munsell Soil Color Charts (2009) during the summers of 2018 and 2019. A total of 414 sediment samples were collected at intervals of 27 cm on average from the trenches (Figure 2). The three sections represent a total sediment thickness of 112.5 m (45.8 m at T1, 26 m at T2, and 50.5 m at T3). In addition, three sediment samples were collected from two prominent, laterally consistent white beds (termed "white marls" by Barbour et al. (1926)) along the Dachangliang ridge between 100 and 330 m further SE of the southernmost section T2 (Figure 1).

3.2 Age constrains of the investigated sediments

To roughly estimate the period of sediment formation represented by the newly investigated sections, we correlated our sections from Dachangliang with the adjacent Palaeolithic artefact-bearing sections Majuangou (MJG), Banshan (BS), and Xiantai (XT) recognized for their established magnetostratigraphic data (Zhu et al., 2004; Ao et al., 2010b). These artefact-bearing sections with established magnetostratigraphy are located relatively closely to the newly investigated sections, in a distance of 100 m (XT) to 800 m (MJG and BS; Figure 1). To determine the age of the sediments at different depths within the studied sections, we compared them to the sediments of nearby sections based on field observations including their sediment colour and grain size, and magnetic susceptibility data. The close proximity of the sedimentary section T2 to the XT section permitted a relatively straightforward stratigraphic correlation, also considering uncertainties due to lateral variations in sedimentary facies. The artefact-bearing bed at XT probably correlates with the sediments in the upper part of section T2 (Figure 12). At MJG, a package of three distinctly coloured sediment layers, characterised as red, gray and yellow (RGY), was noticed. This RGY sediment package was used to laterally trace the four artefact-bearing beds from MJG and one artefact-bearing bed from BS to their correlative intervals at section T3 (Yang et al., 2022; Figure 12). As a result of this correlation, a sediment accumulation rate of ca. 46 ka/m was roughly calculated. Thus, our investigated composite sedimentary section was probably formed within an age constrain between ca. 1.7 and 0.9 Ma, covering

FIGURE 2
Exposed sediment sections T1 to T3, including white marker layers W1, W2 and W3. The thicknesses of T1 and T2 are indicated and the dividing Youfang Fault (broken blue line) which caused a vertical displacement of approximately 30 m. The Sanggan River is flowing in the valley located N of the sampling locations (in the background).

the time from the end of the Olduvai and including the Jaramillo polarity subchrons (Figure 12).

3.3 Laboratory analysis

3.3.1 Grain-size analysis

The grain-size distribution of all collected sediment samples was determined using a Malvern 2000 laser particle size analyzer at the Key Laboratory of Western China's Environmental Systems at Lanzhou University. In preparation for grain-size analysis, samples were chemically digested by sequential addition of HCl and H_2O_2 until carbonates and organic matter were eliminated. Then, the samples were treated with Na-hexametaphosphate to disperse aggregates. At least three measurement runs were performed for each sample, and the average was taken as the final result. The exported grain-size data were processed for sediment classification using the GRADISTAT software package (Blott and Pye, 2001), and the main textural parameters (mean and median grain size, sorting (σ_G), skewness (SK_G) and kurtosis (K_G)) were calculated according to the equations of Folk and Ward (1957). The statistical coding program R language version 4.1.3 was used to identify the main types of grain-size-frequency curves of all samples, and to graphically present the calculated grain-size parameters, and the percentage abundances of the clay, silt and sand fractions *versus* section height (http://www.rstudio.com/). The sedimentological zones of the investigated sections were determined using the change point detection option in the software PAST. This method was selected as it offers a robust and objective way of recognizing changes in sedimentological characteristics and facilitates a precise stratigraphic correlation between the sections.

3.3.2 Magnetic susceptibility

The magnetic susceptibility was measured using SM150L magnetic susceptibility meter (Institute of Earth Sciences, University of Iceland). The samples were first air-dried at room temperature in the laboratory for some days to avoid any chemical reactions. A sub-sample of ca. 10 g was placed in a non-magnetic polystyrene plastic container and measured within an AC magnetic field amplitude of 80 A m^{-1} at a low (χ_{LF}, 500 Hz) and high (χ_{HF}, 4,000 Hz) frequency to calculate the frequency-dependent magnetic susceptibility (χ_{FD}) expressed as percentage χ_{FD} (%) = [($\chi_{LF}-\chi_{HF})/\chi_{LF}$] x 100. A total of six repeat measurements per sample were performed to obtain accurate data and identify outliers.
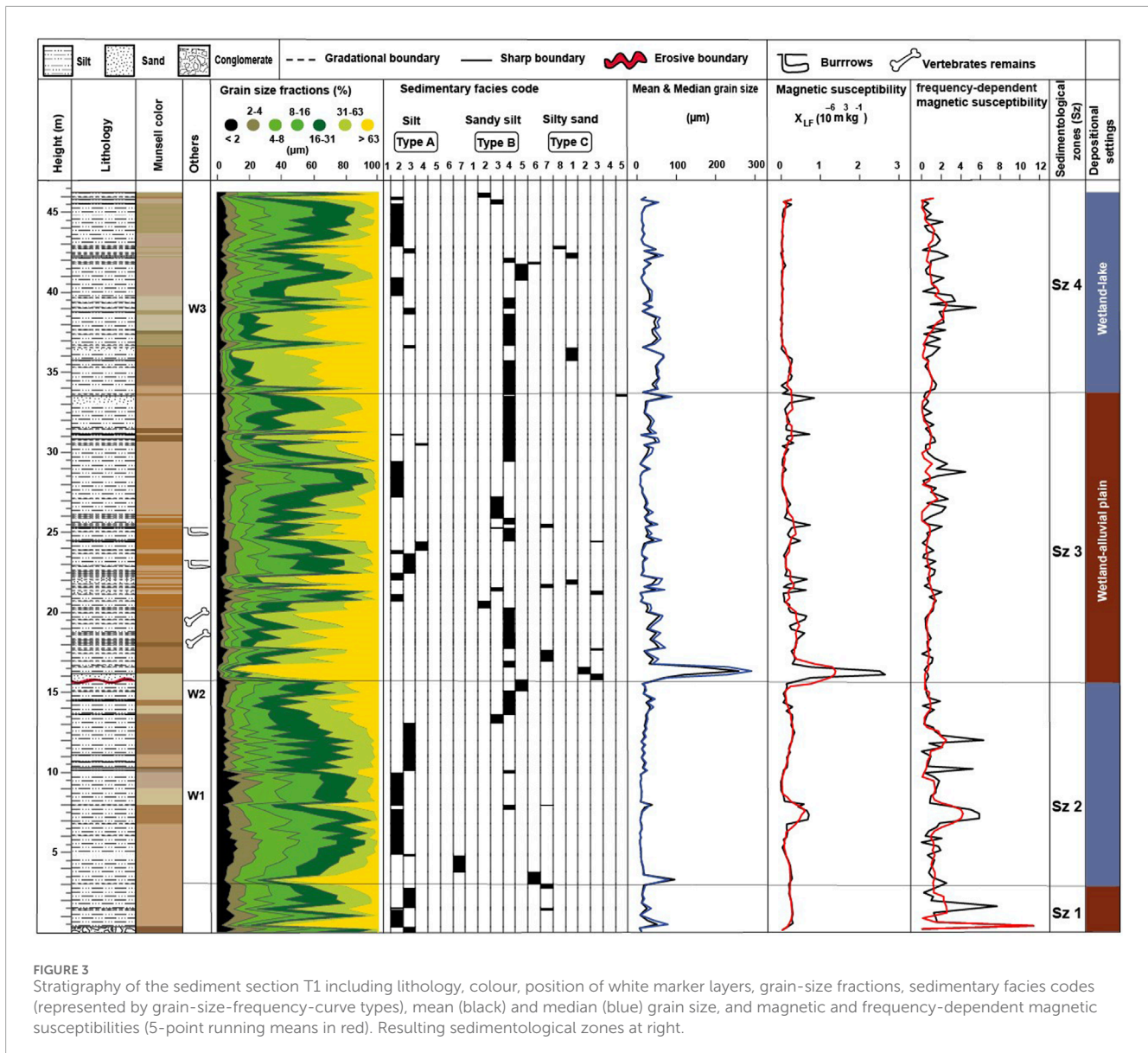
3.3.3 Micropalaeontological analysis

A set of 47 sediment samples, three from individual sample locations in the SE of section T2, 21 from section T1 and 23 from section T3, were selected from two prominent sedimentary beds of white marls and from the under- and overlaying beds at intervals of 2.5 m for micropalaeontological analysis. Sub-samples of 30 g were treated using 3% H_2O_2 for about 24 h to remove organic matter and disaggregate the material. Then, the sediment was washed through standard sieves of 100, 250 and 1000 µm meshes and sieve residues were dried afterwards at 50°C for 24 h. Ostracods were handpicked with needles and brushes from the sieve residues and examined under an OLYMPUS SZ61 low-power binocular microscope. Selected valves of each species were gold-coated and photographed with a Hitachi TM3000 scanning electron microscope. The ostracod valves were identified based on their outline and surface ornamentation according to Mischke et al. (2006) and Pang et al. (2015).

4 Results

4.1 Field observations

The exposed sediments at the sediment sections T1, T2 and T3 are lithologically mostly relatively homogeneous. They partly contain laminations of various thickness, horizontal and ripple bedding, and bioturbation features. The sediments are predominantly composed of varicoloured silt-sized materials, which

FIGURE 3
Stratigraphy of the sediment section T1 including lithology, colour, position of white marker layers, grain-size fractions, sedimentary facies codes (represented by grain-size-frequency-curve types), mean (black) and median (blue) grain size, and magnetic and frequency-dependent magnetic susceptibilities (5-point running means in red). Resulting sedimentological zones at right.
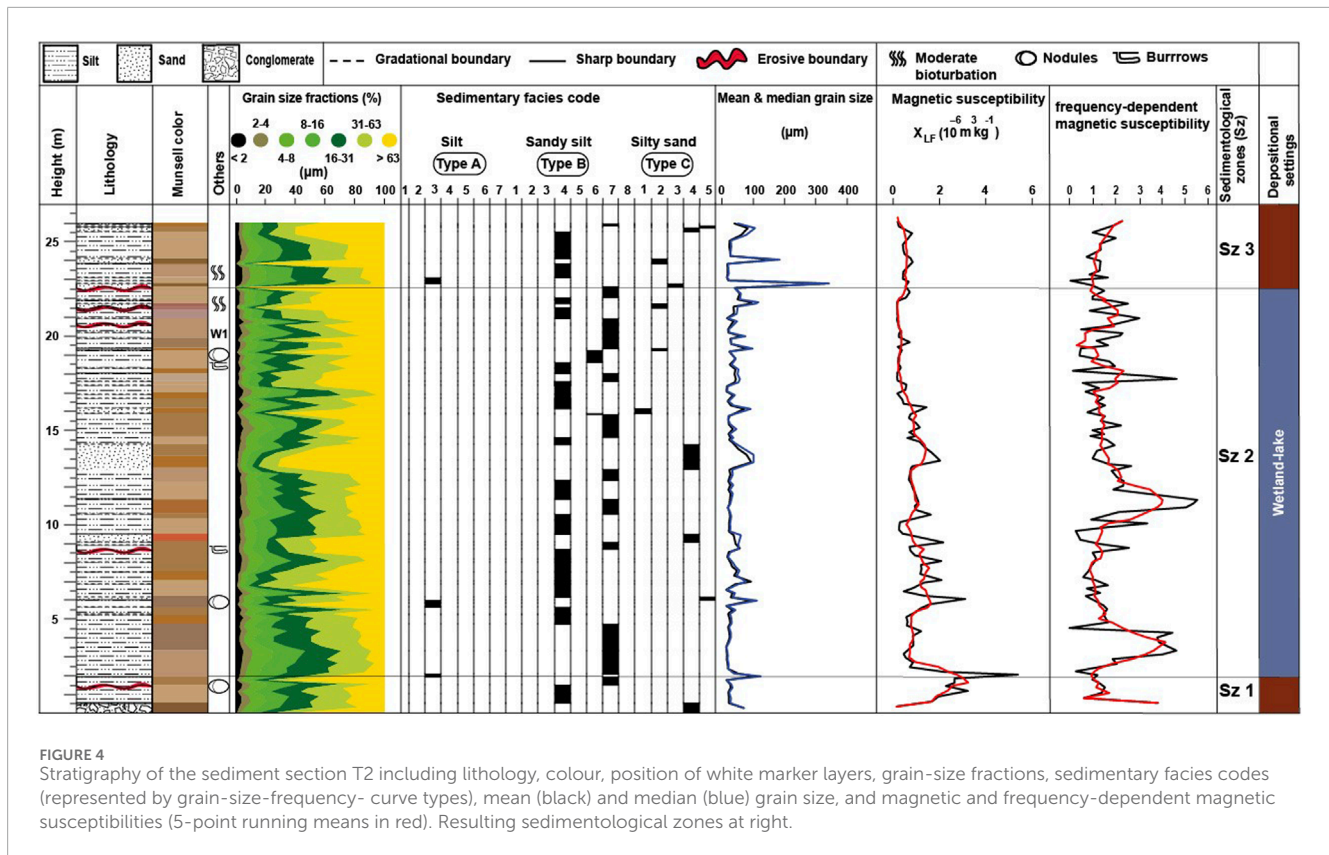
are partly carbonate-rich, and partly interbedded with fine-grained sand layers and minor contributions of clay-sized particles. Carbonate-rich layers, which are up to a centimetre in thickness are occasionally present in the silt deposits. Lithological changes in the stratigraphic sequences occur as transitional, sharp, or erosional boundaries. The sediments display a range in colour on a centimetre scale from mostly very pale brown (10YR 7/3-4), yellowish brown (10YR 5/4-8), light olive gray (5Y 6/2), brownish yellow (10YR 6/8) to more minorly pale yellow (2.5Y 7/3-4), pink 2.5YR 8/3-4), light grey (2.5Y 7/1-2), white (2.5Y 8/1), greyish brown (2.5Y 5/2), reddish brown (2.5YR 4/3-4) and light brown (7.5YR 6/3-4; Figures 3–5).

4.2 Laboratory results

The grain-size analysis of T1, T2 and T3 sediments reveals that coarse-grained silt (16–63 µm) represents the largest sediment

fraction, ranging from a minimum of 4.6% to a maximum of 64%, with an average of 40%. The >63 µm size fraction also represents a significant portion of the sediments, ranging from a minimum of 0.6% to a maximum of 92%, with an average of 23%. The percentage of fine-grained silt (2–16 µm) varies from a minimum of 4% to a maximum of 72%, with an average of 33%. The clay-size fraction (<2 µm) represents the smallest portion; its range is from 0.2 to 15% with an average of 5% (Figures 3–5). The grain-size-frequency distribution for most of the samples (72%) is unimodal, while the remaining samples (28%) show either bimodal or weakly polymodal distributions. The sediments range in mean (and median) grain size from a minimum of 6.3 µm (6.4 µm) to a maximum of 258.9 µm (292.1 µm) with an average of 27.8 µm (32.9 µm) in the T1 sediments, from 16.0 µm (17.0 µm) to 330.6 µm (343.8 µm) with an average of 41.3 µm (47.6 µm) in the T2 sediments, and from 6.7 µm (7.1 µm) to 125.9 µm (149.1 µm) with an average of 20.2 µm (24.1 µm) in the T3 sediments. The sorting (σ_G) values are slightly variable

FIGURE 4
Stratigraphy of the sediment section T2 including lithology, colour, position of white marker layers, grain-size fractions, sedimentary facies codes (represented by grain-size-frequency- curve types), mean (black) and median (blue) grain size, and magnetic and frequency-dependent magnetic susceptibilities (5-point running means in red). Resulting sedimentological zones at right.

from 2 to 10.8 μm (avg. of 3.1 μm) in T1, from 2.1 to 5.5 μm (avg 3.4 μm) in T2, and from 2.4 to 6.7 μm (avg 3.4 μm) in T3 samples, while the skewness (Sk_G) values are between −0.6 and 0.2 μm (avg −0.2) in T1, -0.3 to −0.1 (avg −0.2) in T2 s, and −0.4 to −0.02 (avg −0.2) in T3 samples. Additionally, the investigated samples exhibit kurtosis (K_G) varying from 0.8 to 2.2 μm with an average value of 1.2 μm, whilst T2 and T3 samples have a range between 0.8 and 1.9 μm (avg 1.1 μm), to 0.7–1.9 μm (avg 1 μm), respectively (Figures 6–8). Magnetic susceptibility (χ_{lf}) in the sediment sections varies widely, with a range of 0.1–2.7 x 10^{-6} m³ kg⁻¹ in T1, 0.1–5.3 x 10^{-6} m³ kg⁻¹ in T2, and 0.1–4.4 x 10^{-6} m³ kg⁻¹ in T3. The average χ_{lf} values of the T1, T2 and T3 sections are 0.3 x 10^{-6} m³ kg⁻¹, 0.8 x 10^{-6} m³ kg⁻¹, and 0.7 x 10^{-6} m³ kg⁻¹, respectively (Figures 3–5). The related χ_{FD} values vary between 0.0–11.4%, with an average of 1.3%; between 0.0–5.5%, averaging 1.7%; and between 0.0–44.7%, with an average of 3.4%, respectively.

A freshwater-ostracod assemblage with low diversity is recorded in the three sediment sections with a total of 13 taxa identified. The most abundant species are *Limnocythere flexa*, *Ilyocypris* spp., *Leucocythere* sp. and *Heterocypris salina* (Figure 9). In contrast to slightly darker and coarser-grained sediments, the white marl layers contain abundant valves of *Cytherissa lacustris* apart from the white marl of section T2. The white marls contain less valves of *Leucocythere dorsotuberosa* in comparison to the slightly darker and coarser-grained sediments (Figure 9).
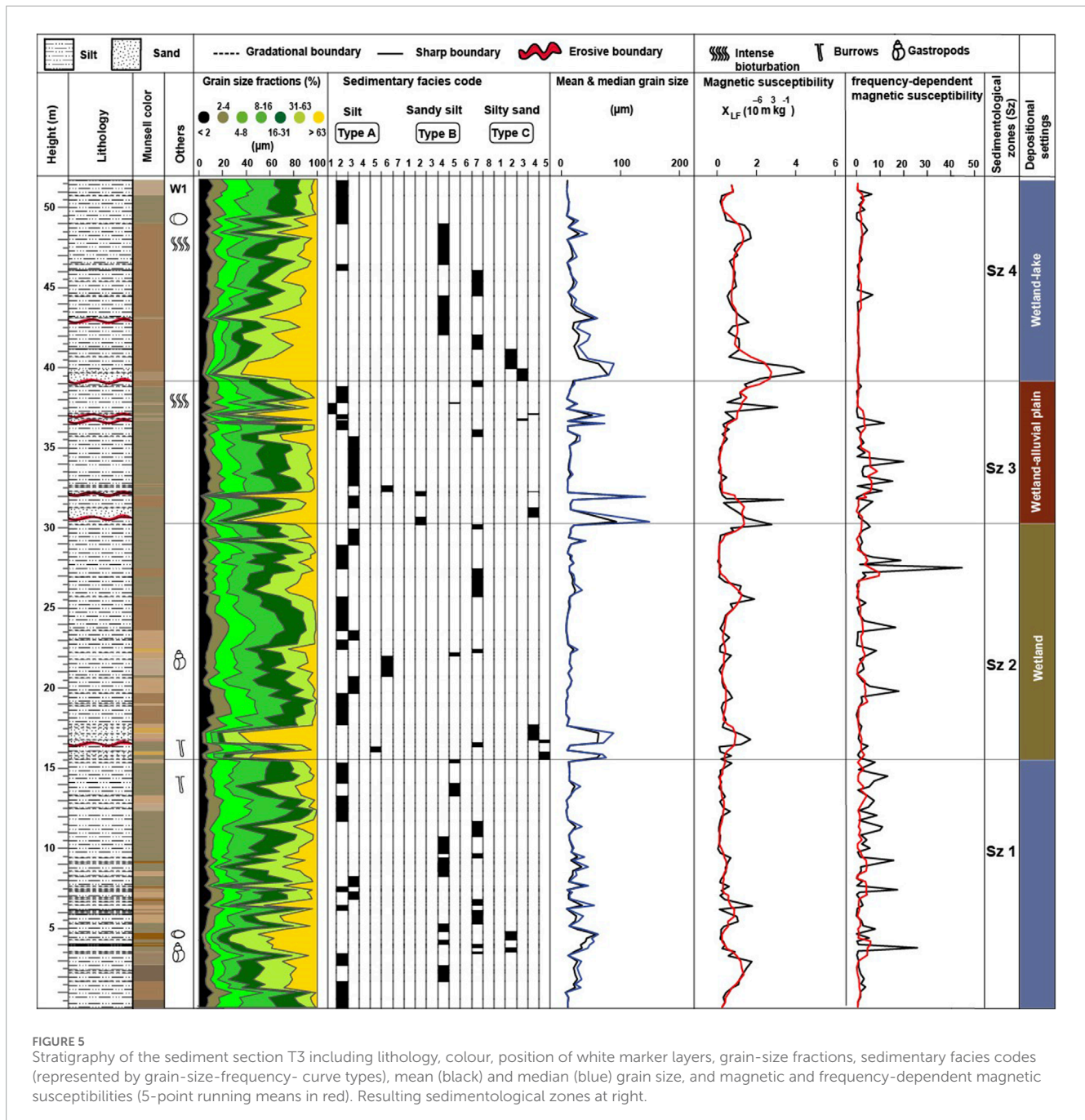
5 Discussion

5.1 Stratigraphic correlation of Dachangliang sediments

Generally, there are no consistent patterns of vertical variations in colour, grain-size distribution or the grain-size parameters sorting, skewness or kurtosis, and MS and χ_{FD} values observed across the three sediment sections (T1-T3). However, a clear differentiation based on sediment type, bedding structures and ostracod assemblage is noticeable (Supplementary Tables S1–S3; Figures 3–8).
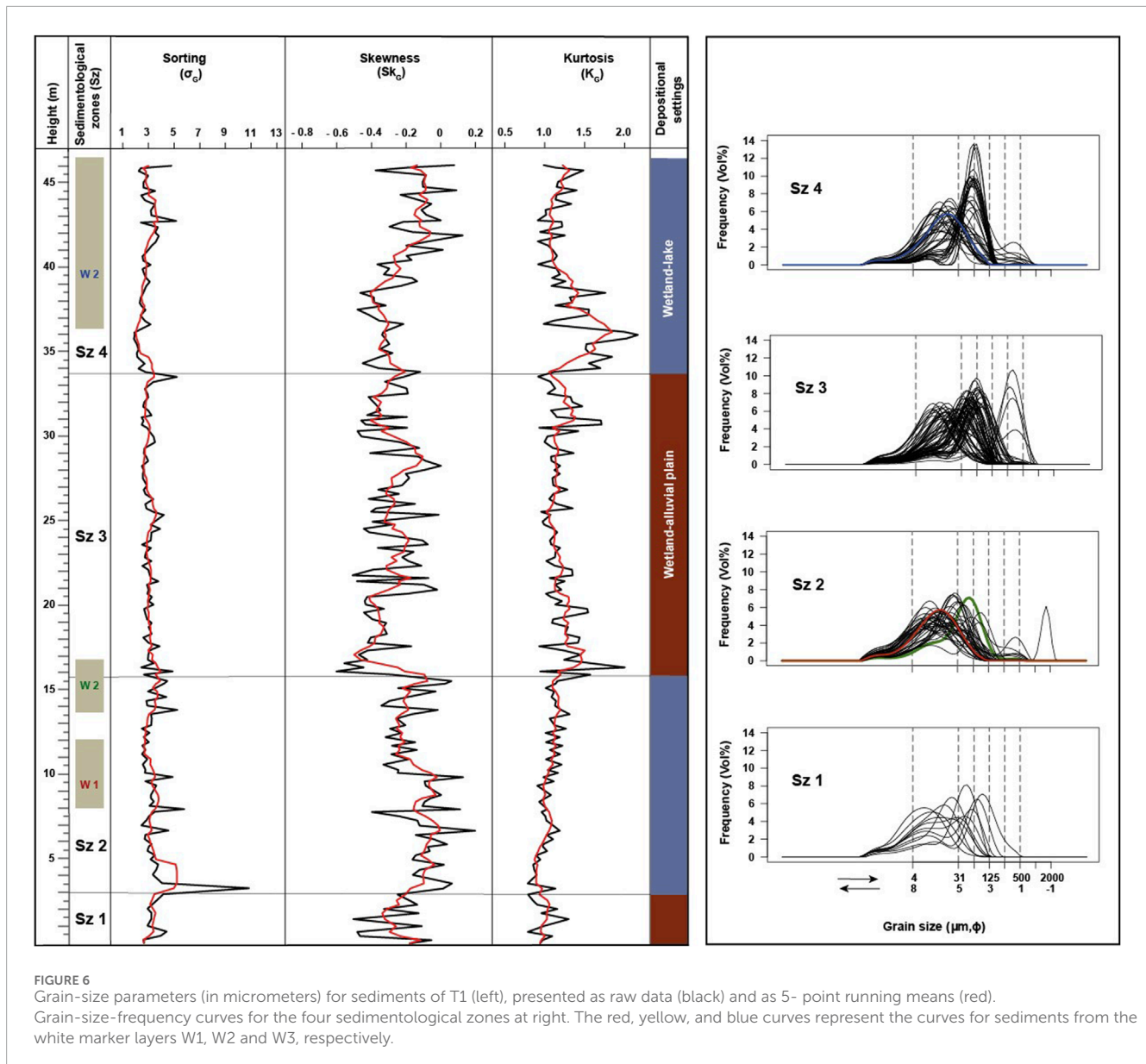
5.1.1 Section T1

In the T1 section, four sedimentological zones were identified (Figures 3, 6):

Sedimentological zone (Sz) 1 (0.0–3.0 m) shows a range of mean grain sizes from fine to very coarse silt, (mostly fine silt from 10.7 to 15.6 μm). The sediments are predominantly characterized by unimodal GSDs with occasional occurrence of bimodal ones. The fine fraction (modes at 4.5–11.7 μm) represents the dominant pattern of these GSDs. The sediments are very poorly to poorly sorted, positive (fine-grained) skewed, and mesokurtic. They are partly structureless and show occasional horizontal lamination at 1.4–3.0 m above base. At the base is a 0.4-m thick gravel layer. The recorded ostracod assemblage is dominated by *Limnocythere* sp., and the presence of *H. salina* probably indicates that sediments

FIGURE 5
Stratigraphy of the sediment section T3 including lithology, colour, position of white marker layers, grain-size fractions, sedimentary facies codes (represented by grain-size-frequency- curve types), mean (black) and median (blue) grain size, and magnetic and frequency-dependent magnetic susceptibilities (5-point running means in red). Resulting sedimentological zones at right.

formed partly in small temporary water bodies (Meisch, 2000). The sediments of *Sz 1* are interpreted as result of fluvial reworking of fine-grained materials of aeolian origin in a densely vegetated paludal environment representing a wetland-alluvial plain depositional setting (cycle 1). The gravels at the base probably resulted from a peak-flow event and the upper sediments of the zone likely represent the settling of fine suspended sediments in a standing water body on the floodplain (Vandenberghe, 2013). The fine-grained characteristics of most of the sediments of *Sz 1* are in remarkable contrast to the relatively pronounced relief at the margins of the Nihewan Basin today, the nearby exposure of bedrock as potential source of sediments and the gravelly deposits in the Sanggan River
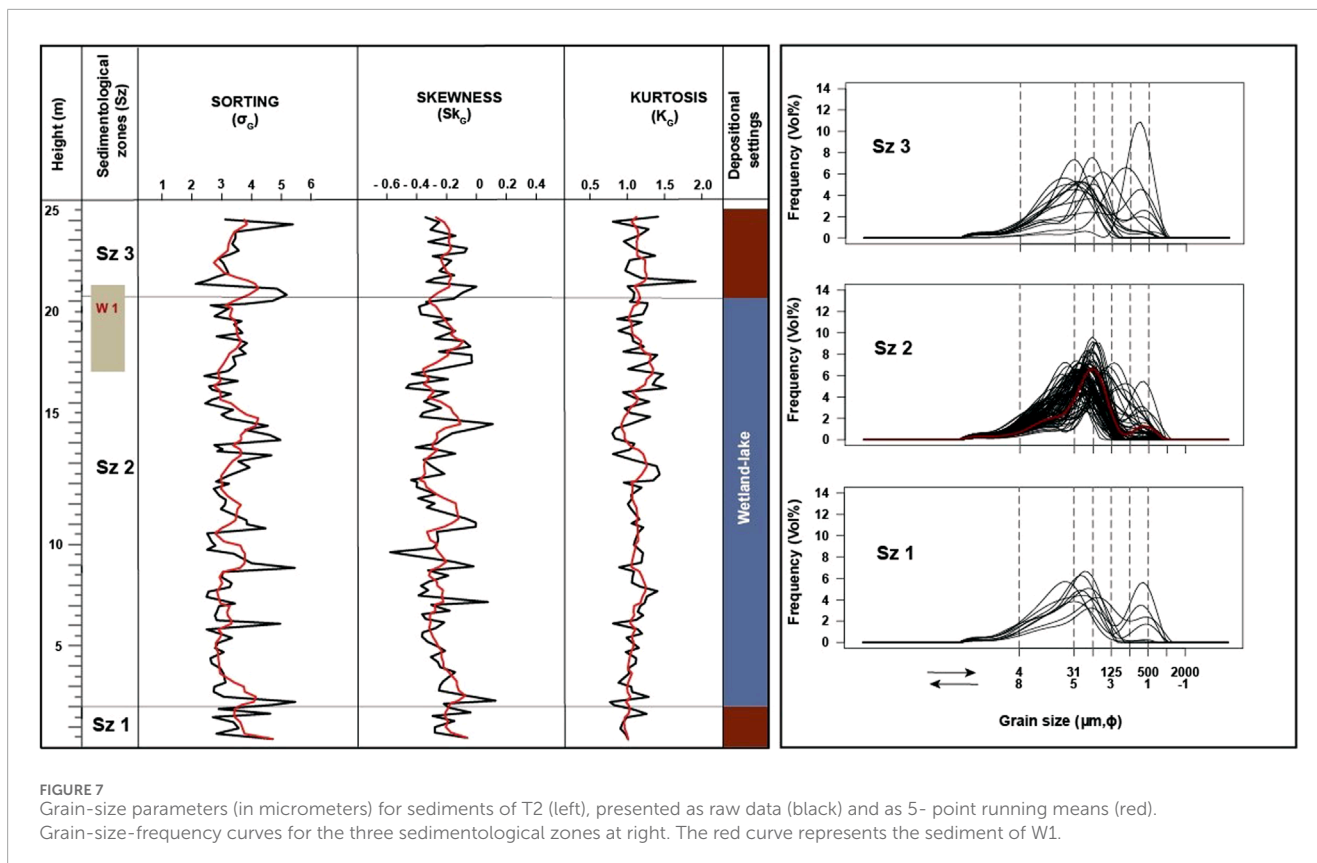
and in the seasonal streams today. The mean grain size of these fine-grained sediments of the zone is comparable to the mean grain size of typical loess sediments that vary between 2–25 μm and were called "small dust" by Stuut et al. (2009) and loess type 1. c by Vandenberghe (2013). These fine-grained loess deposits characterize part of the Red Clays in China (Lebbink, 2010). Sun et al. (2018) suggested that loess deposition in NE China began during the early Pleistocene at ca. 1 Ma. According to Liu et al. (2018) the earliest Nihewan Formation sediments were sourced from Early Pliocene Red Clay deposits that were inferred to originate from weathering of aeolian deposits. Noticeably, some samples from T1-section show similar skewness and grain-size patterns as the Red Clay samples

FIGURE 6
Grain-size parameters (in micrometers) for sediments of T1 (left), presented as raw data (black) and as 5- point running means (red).
Grain-size-frequency curves for the four sedimentological zones at right. The red, yellow, and blue curves represent the curves for sediments from the white marker layers W1, W2 and W3, respectively.

collected from Lingtai at the S CLP (Sun et al., 2006b; Figure 10). Additionally, Yang et al. (2019) inferred the partial aeolian origin for the stone artifacts-bearing silt deposits of fluvial terraces of the Hanjiang River at the S margin of the Qinling Mountains, central China.

The mean grain size of sediments of the *Sz 2* (3.0–15.5 m) is in a range from fine silt to very fine sand (predominantly medium silt from 8.0 to 29.2 μm). Unimodal GSDs are dominant in the sediments of this zone and bimodal distributions occur occasionally. The GSDs of the sediments consist of a higher portion of the fine fraction (modes at 7.4–22.6 μm) and a lower portion of the coarse fraction (modes at 41.1–64.5 μm). The sediments are poorly sorted, and predominantly positive skewed with mesokurtic GSDs. Sedimentary structures are partially present within the zone and include horizontal and ripple lamination and horizontal bedding. Otherwise, the sediments are massive, and deposition probably occurred on a wetland. The sediments at 8.0–12.1 m (W1)

and 13.7–15.8 m (W2) heights are brighter coloured and partly carbonate-rich. Similar brighter and carbonate-rich deposits were already recognized as prominent beds by Barbour et al. (1926) and called "white marls". These sediments are characterized by a relatively higher concentration of ostracods (Figure 9). As in *Sz 1*, *Limnocythere* sp. remains the dominant ostracod taxon, followed by *Cytherissa lacustris* which typically inhibits deep, cold lakes (Meisch, 2000). The horizontal lamination and bedding in *Sz 2*, and the absence of *H. salina* in contrast to *Sz 1* probably indicate a periodic sedimentation of fine and coarse-grained reworked aeolian deposits in a relatively larger water body in comparison to *Sz 1*. The deposition of white marl sediments likely occurred during a period when a lake was present at the location of the section. In contrast to *Sz 1*, the occurrence of coarse-grained sediments with modes of GSDs at 41.1–64.5 μm are comparable to the "large dust" of Stuut et al. (2009) and loess type 1. b of Vandenberghe (2013) which are characterized by modes at 25–65 μm. The coarser

FIGURE 7
Grain-size parameters (in micrometers) for sediments of T2 (left), presented as raw data (black) and as 5- point running means (red).
Grain-size-frequency curves for the three sedimentological zones at right. The red curve represents the sediment of W1.

sediments occur less often and they represent fluvially transported, local materials. Thus, the sediments in *Sz 2* are interpreted as fluvially reworked, originally aeolian deposits which partly accumulated in a wetland and in a lake (cycle 2).

The mean grain sizes of sediment samples from *Sz 3* **(15.5–33.7 m)** range from fine silt to medium sand (mostly medium to coarse silt within 16.3–57.5 μm). Most of the sediments in this zone are marked by the predominance of unimodal GSDs, and bimodal distributions occur occasionally. The sediments are composed of a higher portion of the fine fraction (modes at 7.4–22.6 μm) and a lower portion of the coarse fraction (mode at >65 μm). The sediments are poorly sorted, strongly positive skewed and leptokurtic. As in *Sz 2*, horizontal lamination and bedding structures are evident, and cross bedding occurs at 15.8–16.6 m. An erosional surface is distinct near the base of the zone. The sediments of this zone are otherwise massive. They contain fossil bones and preserve traces of burrows left by animals which indicate that the deposition was under wetland conditions. The ostracod assemblage is slightly more diverse in comparison to *Sz 2*, and the ostracod concentration is lower. The distinctly increased abundance of *Ilyocypris* sp. probably indicates the presence of small ponds and/or slowly flowing streams (Meisch, 2000). Based on the sedimentary characteristics and the ostracods, *Sz 3* can be distinguished into two parts that represent more fluctuating conditions first and more stable conditions afterwards. In the lower part (15.5–30.0 m), the dominant massive beds indicate the deposition in a wetland. However, the occurrence of ripple lamination with ostracods such as *Limnocythere* sp. and very few valves of *C. lacustris* indicate

sporadically occurring fluvial reworking of locally sourced coarse-grained aeolian deposits and accumulation of transported sediments in a larger water body. The upper part (30.0–33.7 m) is characterized by the presence of horizontal bedding and *Leucocythere* sp. which indicate sediment deposition in small water bodies within a distal floodplain environment. These inferred conditions of *Sz 3* could be a result of the deposition in a wetland-alluvial plain setting (cycle 3). The presence of shallow freshwater bodies in this context may have served as a habitat for mammals and their predators. The GSDs of the sediments with mode at >65 μm resemble the modal sizes of nearshore components (C4, C5 and C6) identified in the sediments of Hulun Lake, Inner Mongolia (Xiao et al., 2012).

The mean grain size of sediments in the *Sz 4* **(33.7–46.1 m)** varies from fine silt to very fine sand (dominantly medium to coarse silt within 15.8–58.9 μm). Unimodal GSDs prevail in the zone and bimodal distributions occur occasionally. The sediments typically contain a larger fine fraction (modes at ~7.9–22.8 μm) and a smaller coarse fraction (modes at 41.5–65.0 μm). The sediments show poor sorting, and are dominated by positive skewed, and leptokurtic distributions. As in *Sz 2*, horizontal lamination and bedding structures are also observed in *Sz 4*. However, the sediments are mostly homogenous. A brighter-coloured layer at 36.4–46.0 m (W3) above the base contains micritic carbonate. These observed carbonate-rich sediments of the zone represent the third and thickest white marl layer of the section T1. The number of ostracod taxa in *Sz 4* is slightly higher and concentrations are also higher than in the previous two zones. *Cytherissa lacustris* occurs at 40.9 m and indicates sediment
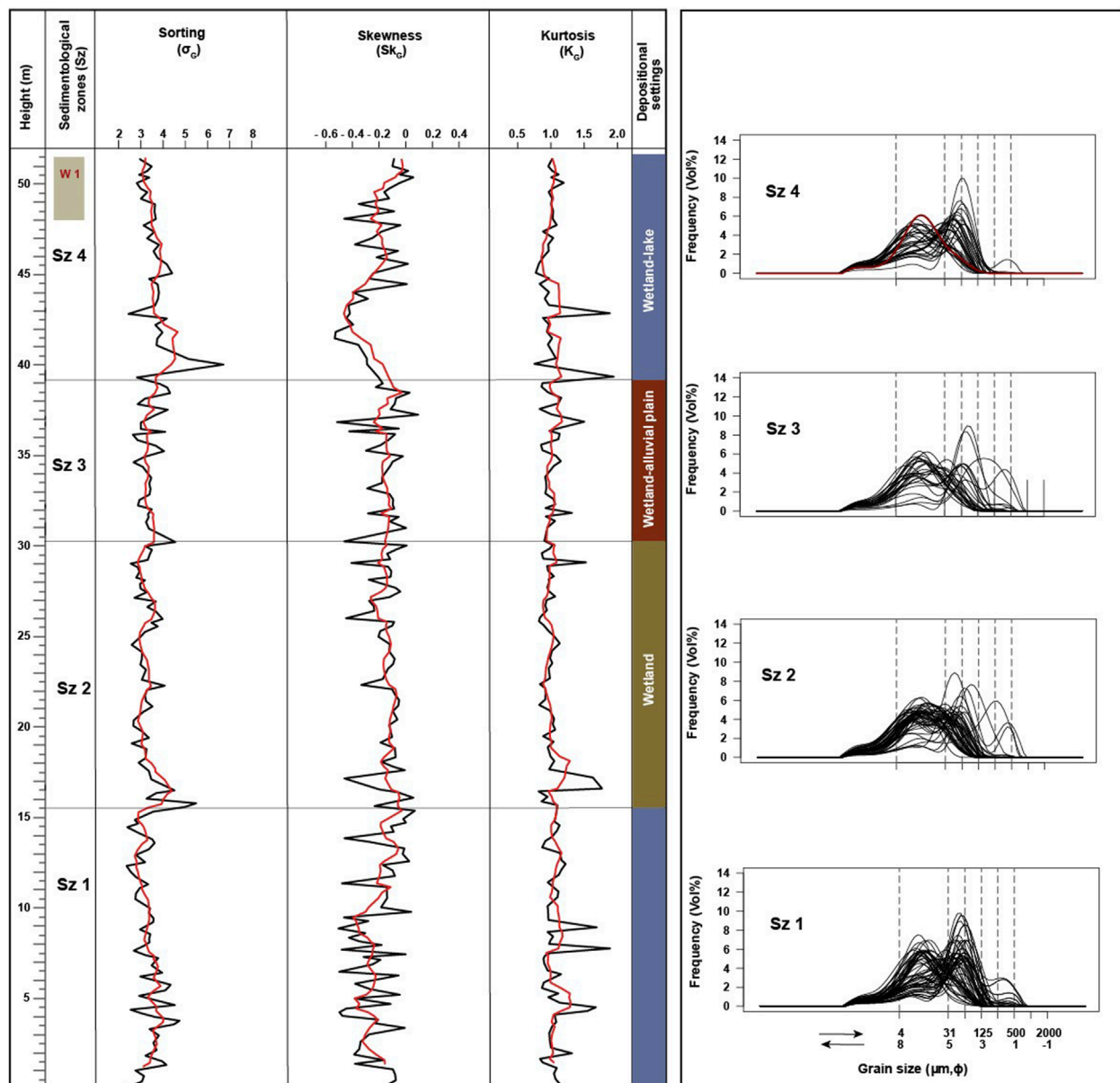
FIGURE 8
Grain-size parameters (in micrometers) for sediments of T3 (left), presented as raw data (black) and as 5- point running means (red). Grain-size-frequency curves for the four sedimentological zones at right. The red curve represents the sediment of W1.

deposition in a deeper freshwater lake. Valves of Candoninae occur at the same depth, and their members occur in various types of water bodies including lakes and wetlands, often characterised by freshwater and cold conditions (Meisch, 2000). The larger mean grain size of sediments of *Sz 4* indicates that sediments accumulated in a setting with higher energy level in contrast to *Sz 2*. *Ilyocypris and Leucocythere* with low numbers in the lower part of the zone suggest sediment deposition in smaller water bodies on a floodplain. Moreover, a longer, stable period with stagnant waters and carbonate precipitation is inferred from the white marls including a period of sediment accumulation in a deeper lake. Thus, a wetland-lake setting is inferred for *Sz 4* (cycle 4).

5.1.2 Section T2

In the T2 section, three sedimentological zones were identified (Figures 4, 7):

The range of mean grain sizes in *Sz 1* **(0.0–2.2 m)** varies from coarse silt to very fine sand (mostly medium silt from 24.9 to 30.2 µm). The sediments are dominantly characterized by unimodal GSDs with occasionally occurring bimodal distributions. The fine fraction (modes at 14.1–25.8 µm) comprises the dominant component of these GSDs. The sediments are poorly sorted, positive skewed, and mesokurtic. No sedimentary structures are found. At the base of the zone is a 0.6-m thick gravel layer. The presence of carbonate nodules is recorded in the sediments. A distinct erosional surface can be observed near to the top of the zone. The recorded
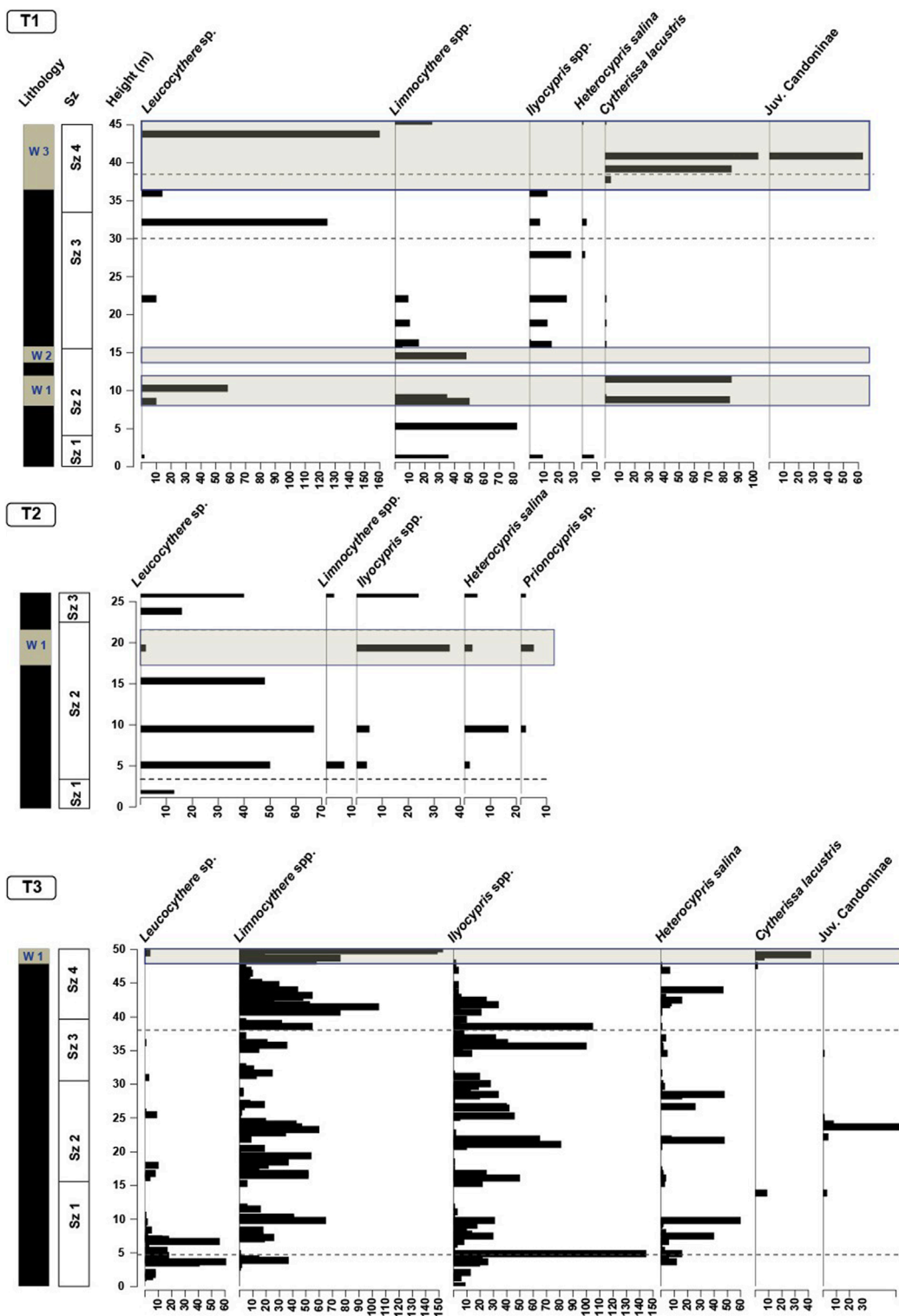
FIGURE 9
Absolute abundances of ostracod valves per 30 g of sediment recorded at the sediment sections T1 to T3. Valves of *Leucocythere* spp. include those of *L. dorsotuberosa*, and valves of *Limnocythere* include those of *L. flexa*. Gray horizontal bars indicate the white marker layers.

ostracod assemblage is only represented by *Leucocythere* sp., a taxon possibly adapted to cold climate and rapid hydrochemical fluctuations (Mischke et al., 2006). Valves of *Leucocythere* were

identified in surface sediments from shallow water depths between 0.2 and 1.5 m in unstable seasonal ponds (Zhang et al., 2013). The presence of massive beds points to the deposition in a
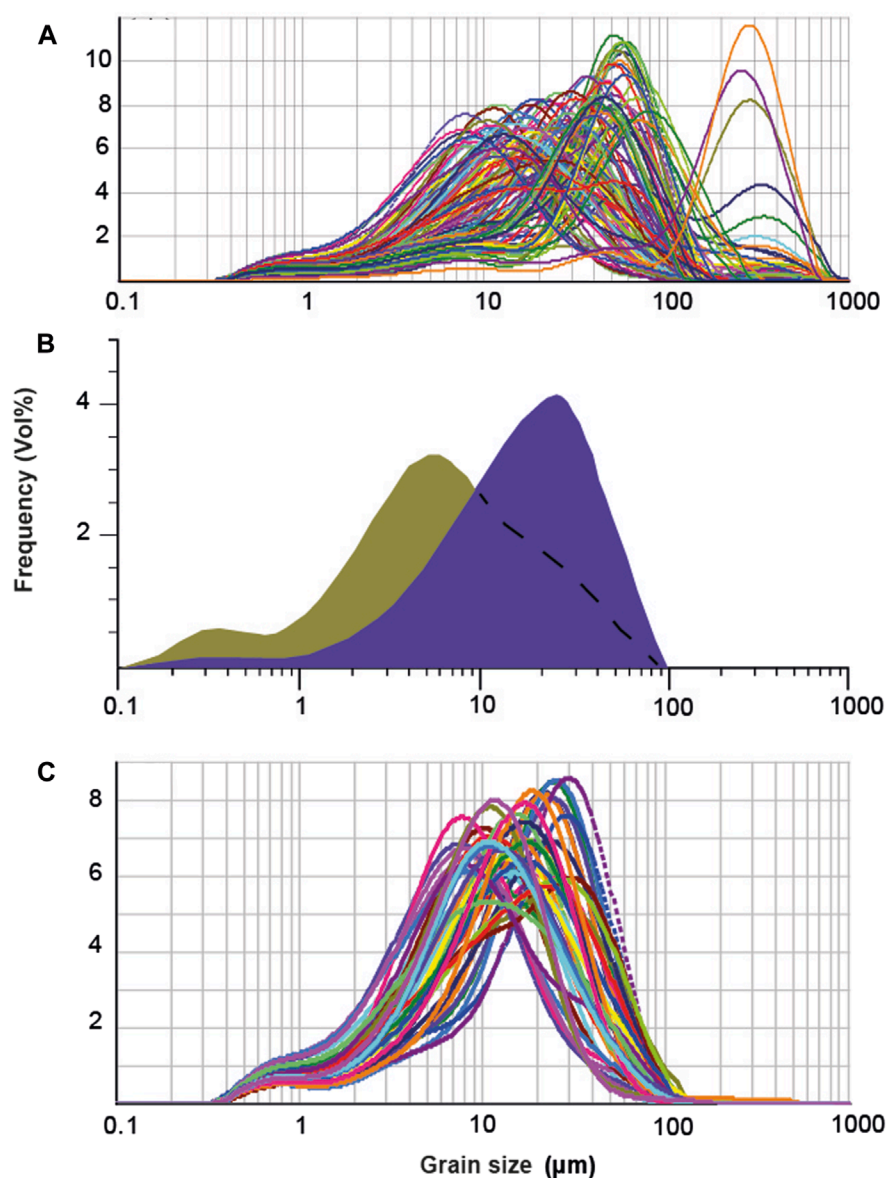
FIGURE 10
(A) Grain-size-frequency curves for sediments from section T1. **(B)** Representative grain-size curve of Red Clay (bulk sample in green, quartz fraction in purple) from Lingtai section, S Chinese Loess Plateau redrawn from Sun et al. (2006b). **(C)** Most abundant modes of grain populations at section T1.

wetland. Nevertheless, the monospecific ostracod assemblage and low abundance of specimens preserved in the sediments of *Sz 1* indicate fluvial reworking of fine-grained materials of aeolian origin on an alluvial plain which experienced subaerial exposure from time to time. Thus, the sediments in *Sz 1* are interpreted to result from accumulation in a wetland-alluvial plain depositional setting (cycle 1).

The sediments of the *Sz 2* **(2.2–22.5 m)** typically have a mean grain size between coarse silt to very fine sand (dominantly medium to coarse silt within 16.0–59.3 μm). Most of the sediments show unimodal GSDs with the occasional occurrence of bimodal distributions. These GSDs are composed of a higher portion of the fine fraction (modes at 5.5–23.2 μm) and a lower content of the coarse fraction (mode at 41.1–62.3 μm). The sediments are

poorly sorted, positive skewed, and they have mainly leptokurtic and mesokurtic distributions. In contrast to *Sz1*, the sediments of this zone show horizontal lamination and bedding, and ripple lamination structures. The sediments at 17.5–21.8 m (W1) are distinguished by its brighter colour and partly carbonate-rich composition which suggest accumulation in stagnant waters. They also contain carbonate nodules, traces of burrows and other evidence of moderate bioturbation. The brighter layer resembles the white marl layers of T1. Four distinctive erosional surfaces are also recognized, representing individual flooding events. The recorded ostracod assemblage predominantly contains *Leucocythere* sp., and also includes *Ilyocypris* sp. and *H. salina*. The presence of *Prionocypris* sp. indicates slowly flowing streams with abundant vegetation (Meisch, 2000). The collective evidence

suggests that the sediments of *Sz 2* are fine and coarse-grained reworked aeolian deposits which were mostly deposited in a more stable, low-energy aquatic setting in comparison to *Sz 1*. Thus, a dominating wetland-lake depositional setting (cycle 2) is inferred which was interrupted from time to time by fluvial conditions.

The mean grain size in the *Sz 3* (22.5–26.0 m*)* varies from coarse silt to medium sand (mostly medium silt from 18.3 to 29.0 μm). Unimodal GSDs prevail, and bimodal distributions occur occasionally. The fine fraction (modes at 14.1–27.6 μm) represents the dominant component of these sediments. The sediments show similar sorting, skewness and kurtosis as those of *Sz 2*. Cross bedding (22.8 m) and horizontal bedding (23.0–25.8 m) occurs but otherwise, sediments are mostly homogeneous. Traces of moderate bioturbation are evident. Ostracod remains are less abundant compared to *Sz 2*, with *Ilyocypris* sp. as the dominant taxon. The deposition of massive beds and the occurrence of few valves of *H. salina* are indication for wetland conditions. Thus, the characteristics of *Sz 3* probably represent sporadic fluvial reworking of fine-grained reworked aeolian materials in a wetland-alluvial plain setting (cycle 3).

5.1.3 Section T3

In the T3 section, four sedimentological zones were identified (Figures 5, 8).

Sz 1 (0.0–15.5 m) shows a range of mean grain sizes from fine silt to very fine sand (mostly fine to medium silt within 8.1–27.3 μm). The sediments are dominantly characterized by unimodal GSDs with occasionally occurring bimodal distributions. These GSDs are composed of a higher portion of the fine fraction (modes at 5.5–20.4 μm) and a lower portion of the coarse fraction (modes at 44–58.5 μm). The sediments are poorly sorted, positive skewed, and mesokurtic. The sediments are mostly homogeneous which is indicative for the deposition in a wetland. However, horizontal and cross bedding sedimentary structures occur at a few stratigraphic levels within the zone. Carbonate nodules and traces of burrows left by animals are common. The sediments also contain gastropod shells and abundant ostracod valves. *Limnocythere* sp. and *Ilyocypris* sp. are the dominant ostracod taxa. The sediments in this zone might have formed under similar depositional conditions as those of *Sz 2* at section T1. Nevertheless, lake conditions at the zone top are marked by the presence of *C. lacustris*. This points to a wetland-lake deposition setting (cycle 1).

The mean grain sizes of sediment samples from *Sz 2* (15.5–30.4 m) range between fine silt to very fine sand (mostly fine silt from 8.1 to 15.3 μm). Unimodal GSDs dominate in this zone and bimodal distributions occur occasionally. The fine fraction (modes at 6.7–17.4 μm) comprises the dominant component of these GSDs. The sediments show similar sorting, skewness and kurtosis to *Sz 1*. The only recognized sedimentary structure is horizontal lamination. However, the sediments are mostly homogeneous and include traces of burrows left by animals which are evidence for wetland conditions. A distinct erosional surface at 16.3 m probably results from a flooding event. The sediments in this zone contain remains of gastropods and a relatively higher concentration of ostracods compared with *Sz 1*. The recorded ostracod assemblage is dominated by *Limnocythere* sp. and *Ilyocypris* sp. Valves of Candoninae and *H. salina* are also present. The collected evidence

indicates a gentle and periodic deposition of reworked fine-grained suspended aeolian materials in a large, shallow and vegetated standing water body on a low-energy alluvial plain environment. Thus, deposition is interpreted to have occurred in a wetland setting (cycle 2).

The mean grain sizes of sediment samples from *Sz 3* (30.4–39.3 m) are within a range from medium silt to fine sand (mostly fine silt from 8.8 to 15.5 μm). Most of the sediments in this zone show unimodal GSDs with the occasional occurrence of bimodal ones. The fine fraction (modes at 6.1–17.6 μm) is the dominant pattern in these GSDs. The sediments show sorting, skewness and kurtosis similar to *Sz 2*. Horizontal lamination, cross bedding and ripple marks are evident. Other sedimentary structures include traces of intensive bioturbation. The ostracod concentration is lower than in *Sz 2*. The recorded ostracod assemblage is dominated by *Limnocythere* sp. and *Ilyocypris* sp. with a significant decrease in the concentration of *H. salina*. This may reflect similar depositional conditions to the sediments of *Sz 1* at section T1. Thus, deposition in a wetland-alluvial plain setting is inferred (cycle 3).

The sediments of the *Sz 4* (39.3–50.5 m) typically have a mean grain size between fine silt to very fine sand (mostly fine silt from 8.7 to 14.8 μm). Unimodal GSDs are dominant with the occasional occurrence of bimodal distributions. These GSDs are dominantly composed of the fine fraction (modes at 5.2–16.6 μm). The sediments show similar sorting, skewness and kurtosis as those of *Sz 3*. Horizontal lamination and ripple marks are found. The sediments in this zone include traces of intensive bioturbation at 46.5 m. The sediments at the height of 48.15–50.85 m (W1), are relatively similar to that was described in *Sz 2* of section T1 as W1 and W2. Moreover, a relatively higher concentration of ostracods is present in these sediments of this zone compared to those of *Sz 3*. The recorded ostracod assemblage is dominated by *Limnocythere* sp. and *Ilyocypris* sp., and *H. salina* is present too. In contrast to *Sz 2*, these sediments were likely deposited in larger and deeper ponds under low-energy conditions in topographically lower areas of alluvial settings. The distinct presence of *C. lacustris* at 49.5 m in the prominent brighter-coloured layer likely represents a period of lacustrine deposition at larger water depth. The majority of the sediments of *Sz 4* were formed in a wetland-lake depositional setting.

5.1.4 White marl deposits

The T1 section contains three distinct white marl layers (W1-W3). They lack bedding structures and are mainly composed of fine groundmass of micritic carbonate. They also contain disseminated angular inorganic detrital constituents (mostly quartz and feldspar grains) with the absence of skeletal grains >1 mm (Figure 11). This supports the in situ-formation of these carbonate-rich sediments. It indicates that these sediments were likely deposited in low-energy aquatic conditions. The marl sediments are, therefore, of lacustrine or paludal origin. The mean grain size of the non-calcareous sediments of W1 is between fine to medium silt (mostly fine silt 8.3–23.0 μm). They are poorly sorted, and the GSDs are mostly positive skewed and mesokurtic. Sediments of W2 show mean grain size between fine to medium silt (mostly medium silt 13.9–29.2 μm). They are poorly sorted, and the GSDs are mostly positive skewed and leptokurtic. The mean grain size of sediments of
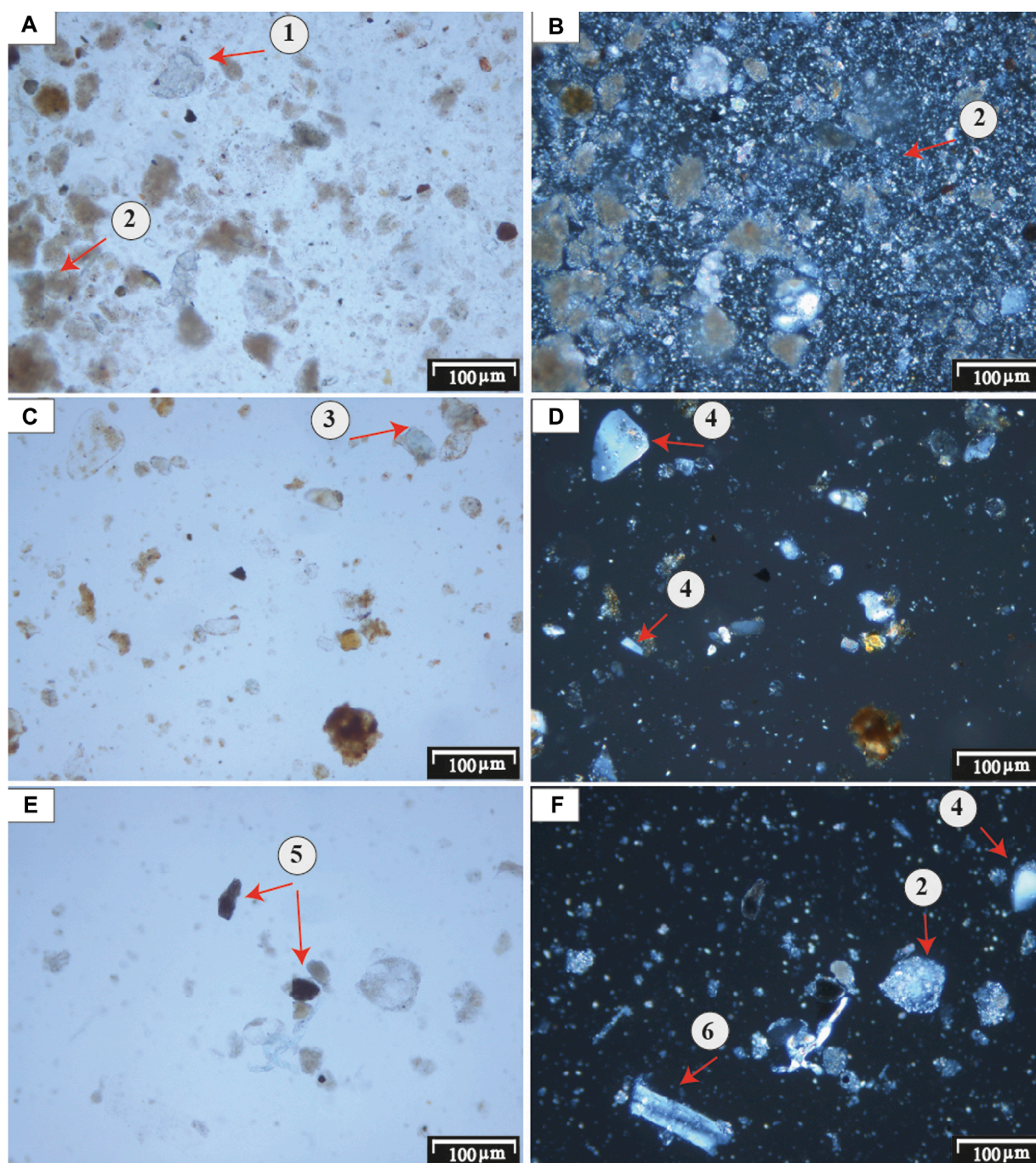
FIGURE 11
Photomicrographs of the mineral constituents encountered in the white layers (W1-W3). All figures were taken at ×50 magnification under transmitted white light. Figures **(A, C, E)** were in plane-polarized light, and **(B, D, F)** were in cross-polarized light. 1) lithoclast of limestone, 2) micritic carbonate 3) carbonate-coated quartz grain or rock fragment 4) quartz grain, 5) rock fragments, 6) weathered feldspar grain.

W3 is between fine to coarse silt (mostly coarse silt 10.8–51.8 μm). It is poorly sorted, and the GSDs are mostly strongly positive skewed and leptokurtic. All three layers show low MS and χ_{FD}. The monospecific assemblage of *C. lacustris* was exclusively recorded in these layers. The ostracod assemblage indicates that the deposition of the marl sediments occurred in a deep lacustrine setting (Meisch, 2000).

In the T2 section, there is a similar white marl layer without bedding structures which represents in situ-formed micritic carbonate. The mean grain size of the layer is between medium silt to very fine sand (mostly coarse silt 18.5–81.8 μm). It is poorly sorted and has mostly positive to strongly positive skewed and leptokurtic GSDs. Also here, the white marl has low MS and χ_{FD}. The recorded ostracod assemblage in this layer is dominated by *Ilyocypris*

sp., accompanied by valves of *Leucocythere* sp.*, H. salina* and *Prionocypris* sp. The assemblage indicates that paludal conditions prevailed during the formation of this white marl layer. We first correlate the T1-T3 sections using their elevations above sea level, specifically the height positions of the white marl layers (Figure 12). The presence of a distinctive erosional surface near to the top of the white layer in T2 can be reasonably correlated with a similar surface near the top of W2 at section T1 which marks a period of significant erosion (Figure 3). Similarly, the base of this layer likely correlates with the base of W1 at section T1 due to the nearly equal thickness of the two layers W1 and W2 in T1. Alternatively, the white marl in T2 could theoretically be correlated to every white marl layer in T1 based on the nearly similar grain size and magnetic susceptibility. The recognized ostracod assemblage of the white marl layers in T1, dominated by either *C. lacustris* or *Limnocythere* spp., differs from the assemblage of the white marl layer in section T2, dominated by *Ilyocypris* spp. (Figure 9). However, such difference possibly results from slight habitat differences within the lake environment during the deposition of the sediments of the sections T1 and T2 which occurred probably less closely spaced than their vicinity implies today assuming that the horizontal component of displacement along the Youfang Fault was not insignificant (Deng et al., 2008; Ao et al., 2013b; Figures 1, 2). The originally larger distance between the accumulation areas of sections T1 and T2 is also supported by the relatively coarser-grained sediments of the section T2 not only in comparison to those of section T1 but also of section T3. We favor the correlation of the white layer in section T2 with layer W1 and/or W2 in section T1 based on the more comparable thicknesses of these layers and their vertical position taking the assumed vertical displacement along the Youfang Fault of ca. 30 m into account (Deng et al., 2008; Figure 12).

The T3 section also contains one distinct white marl layer which does not include bedding structures and constitutes in situ-formed micritic carbonate. The mean grain size is mostly fine silt (8.7–10.8 µm). Sediments are poorly sorted, and GSDs are mostly near symmetrical and mesokurtic. As all the white marl layers, low MS and moderate χ_{FD} were recorded. The ostracod assemblage only contains *C. lacustris* valves which indicate a deep lacustrine depositional environment. This white layer can be easily traced across the sampling location with W1 at section T1 with the absence of erosional surface or any stratigraphic breaks. Furthermore, both show good correlation in the mean grain size and MS patterns (Figures 3, 5). Additionally, the ostracod assemblages are more or less identical and strongly support the correlation (Figure 9). The alternative correlations of the white marl layer in section T3 with W2 or W3 in section T1 have some drawbacks either due to the different topographic position or the significant differences in the ostracod assemblages (Figure 9). In addition, the lithologically distinct and varicoloured beds of the three sediment sections T1, T2 and T3 exhibit lateral continuity in the partially exposed sediments in between these sections along the Dachangliang mountain ridge. Specifically, lateral continuity of the prominent white marl layers, being apparently consistent and correlative throughout sections, permits the T1-T3 sediments to be stratigraphically and lithologically correlated (Figure 12). The ostracod assemblages of the white layers further support the correlation between the T1-T3 sections using the colour of the sediments and the presence of carbonate in these layers. These inferences permit the

establishment of a 86.2-m thick, more or less continuous synthetic composite sedimentary section (NH-T) with six sedimentological zones (Figure 12).

5.2 Depositional cycles and palaeoenvironment of the Dachangliang (DCL) section during ca. 1.7−0.9 Ma

In the study area, the vertical sediment succession of the NH-T section shows minor changes in grain size with recognizable variations in sediment colour, bedding structures, magnetic mineral concentrations, and the presence of ostracods. Therefore, these variations in sediment characteristics and faunal composition suggest a clear vertical sequence of six depositional settings (Figure 13). Thus, the depositional environment at NH-T section represents six cycles of changing hydrodynamic conditions from 1) wetland and lake, 2) wetland, 3) wetland and alluvial plain, 4) wetland and lake, 5) wetland and alluvial plain, and ultimately, 6) wetland and lake. NH-T cycles obey Walther's Law (Walther, 1894) and possibly occurred side-by-side spatially.

The first sedimentary cycle (0.0–15.5 m) represents the dominance of a wetland environment replaced by abrupt episode of alluvial plain (3.5 m) and a shallow ephemeral lake (14.0 m). The second cycle (15.5–30.4 m) marks a distinct period of stable wetland setting. The third cycle (30.4–39.3 m) is a transitional phase of increased fluvial activity and gradual reduction in wetland setting. Sediments of the fourth cycle (39.3–55.8) probably deposited in different environmental conditions of a wetland to shallow ephemeral lake setting including periods of deeper lake facies. The fifth cycle (55.8–74.0) is characterized by a thicker stratigraphic interval of wetland-alluvial plain sediments in comparison with the third cycle. The sixth cycle (74.0–86.2) represents changing conditions from wetland to shallow ephemeral lake settings including periods of deeper lake facies similar to the sedimentary patterns of the fourth cycle.

The general assessment of the late Cenozoic sedimentary evolution of the Nihewan Basin by Chen et al. (2015) implied three stages of rapid expansion, contraction and extinction of the basin during 3.6-2.6, 2.6-1.8 and 1.8-0.11 Ma, respectively. They also suggested that the Pleistocene sediments near the NE margin of the basin were mainly deposited in a braided river (Nihewan Formation, 2.15-1.8 Ma) to alluvial fan environment (Xiaodukou Formation, 1.8-0.2 Ma; Chen et al., 2015). A braided river setting in the region agrees with our inference of mostly wetland conditions at the NH-T section. Nevertheless, the sporadically recorded lake beds show an upward-fining trend from shallower deposits near the section base to deeper and thicker deposits towards the top during ca. 1.7-0.9 Ma. In contrast, Zhu et al. (2004) suggested that the depositional environment at MJG (1.66-1.32 Ma) was lacustrine with brief intervals of wetland and lake-margin settings which is comparable with the inference of wetland and lake facies associations of cycles 1 and 2 at the lower part of NH-T. Both MJG and NH-T sections are located near the E margin of the basin and their sediments are well correlated by three distinctive coloured layers (red, gray and yellow), although our multi-proxy study indicates that sediments
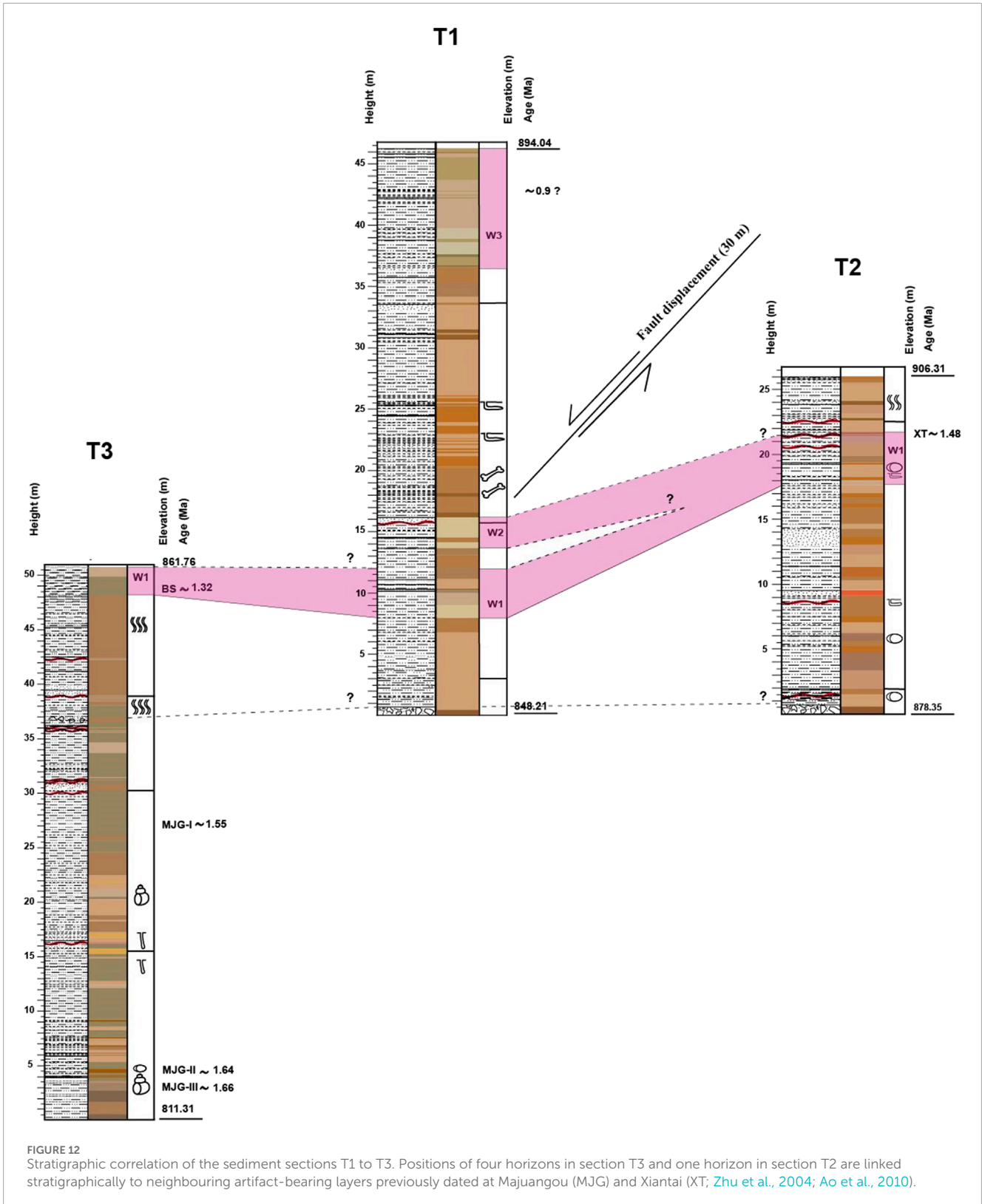
FIGURE 12
Stratigraphic correlation of the sediment sections T1 to T3. Positions of four horizons in section T3 and one horizon in section T2 are linked stratigraphically to neighbouring artifact-bearing layers previously dated at Majuangou (MJG) and Xiantai (XT; Zhu et al., 2004; Ao et al., 2010).

mostly represent wetland deposits rather than prevailing lacustrine conditions (Zhu et al., 2004). Yang et al. (2022) suggested a shallow lacustrine environment during hominin activity (1.324-1.317 Ma) at the Banshan site, which later experienced lake expansion and lake-level rise (1.318-1.310 Ma). This aligns with our interpretation of the facies association of cycle 4, including wetland, shallow and deep lake deposits. Li et al. (2008) investigated the Xiaodukou section in the basin center and also at Donggutuo and Xiaochangliang sections
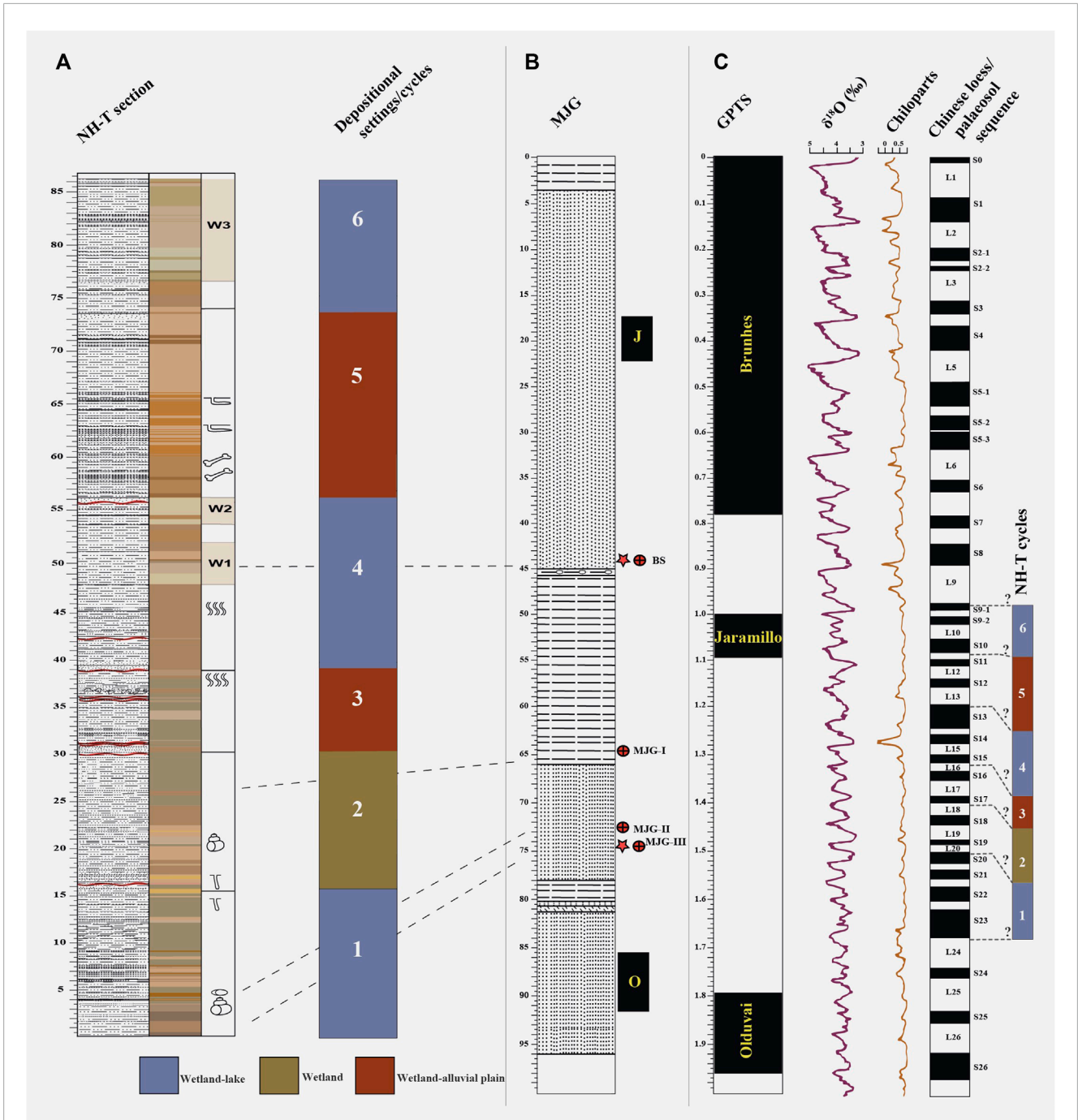
FIGURE 13
(A) Depositional settings in the Nihewan Basin during the Early Pleistocene. **(B)** Stratigraphic section of MJG redrawn from Zhu et al. (2004). **(C)** Geomagnetic Polarity Time Scale (GPTS) by Hilgen et al. (2012), in comparison with climate records in the region: stacked benthic δ^{18}O record (Lisiecki and Raymo, 2005), Chinese loess Chiloparts timescale (Ding et al., 2002), and Chinese loess/palaeosol sequence (L loess, S palaeosol) by Liu et al. (1985).

near the E margin of the basin and inferred a river-dominated to a lake depositional setting for their cycle II which resembles the cycles 5 and 6 of the NH-T section. Bi et al. (2022) inferred that the Datong Basin, located to the W of the Nihewan Basin, underwent a transition from dominant fluvial conditions (7.0-4.2 Ma) to the development of lacustrine environments (4.2-1.8 Ma) due to dip-slip fault activities, and ultimately, a gradual shrinkage of the lake after 1.8 Ma.

5.3 Implications for the reconstruction of early pleistocene climate change in the Nihewan Basin

Considering that the sediments of the NH-T section probably formed between 1.7 and 0.9 Ma, we identified patterns of sedimentary facies types A and B which are indicative of wetter conditions, while facies type C marks drier conditions (Figures 3–5). The three facies types A, B and C are defined on the basis of lithology as silt, sandy silt and silty sand, respectively. The facies code range (1–7) at each type are ascendingly sorted from unimodal to trimodal grain-size distribution curves. Additionally, three dominant fine-to coarse silt-sized components and the ostracod-assemblage changes were observed in the sediments. These observations collectively suggest three distinct cycles 1, 4 and 6 as indicative periods of warmer and wetter climate, whilst cycles 2, 3 and 5 represent three periods of colder and drier climate. The NH-T section is ca. 90 m thick, and sediments likely formed over a period of ca. 800 ka. Assuming that the sediment accumulation occurred relatively constantly without major changes of the depositional rate, sedimentary cycles of 15–20 m thickness may represent periods of roughly 150 ka. Thus, the cycles inferred for the NH-T section possibly represent several long-term climatic fluctuations. In the early Pleistocene, astronomically driven global glacial-interglacial cycles (Milankovitch cycles) had periodicities of ca. 41-ka (Ruddiman et al., 1989). We may speculate that cycles of roughly 150-ka duration at the NH-T section may represent four of such global glacial-interglacial cycles. The Quaternary loess sequences of the CLP recorded long-term glacial-interglacial fluctuations as loess-soil couplets, probably most appropriate to attempt a correlation of the NH-T section with a long-term record of global climate change due to their proximal geographic location in the SW of the Nihewan Basin.

Our detailed assessment of the NH-T sediment characteristics is typically not available for similar sections in the region. Results of the sedimentological analysis indicate only few minor flooding events and do not include significant evidence for high-energy deposits formed in the river channel. These findings suggest that larger parts of the section probably experienced only limited influence by the dynamic changes of the Sanggan River course. Thus, we argue that the sediments are rather indicative of regional climate conditions over the estimated period. The wetland-lake settings inferred from NH-T probably suggest prevailing warm and wetter conditions resulting from a stronger E Asian summer monsoon (EASM). These conditions likely correspond to the interglacial periods S_{23}-S_{20}, S_{15}-S_{13} and S_{10}-S_9 which were previously inferred from paleoclimatic records from CLP (Ding et al., 2002; Figure 13). Conversely, the inferred wetland-alluvial plain settings in the NH-T section are probably contemporaneous with the predominantly cooler and drier conditions of the glacial periods L_{20}-L_{18}, L_{17}-L_{16} and L_{13}-L_{11} (Figure 13). Nevertheless, the occasionally recorded influx of coarsest sediment type C represents brief episodes of the coolest and driest conditions, predominantly observed within the wetland-alluvial plain settings (Figures 3–5).

Meng et al. (2018) studied dolomite and calcite contents of three sediment sections on the CLP as proxies of rainfall-controlled carbonate dissolution to reconstruct EASM rainfall intensity. Their findings show an overall increasing trend of interglacial EASM rainfall from 1.65-0.5 Ma which is apparently supported by our observed upward increases in the thickness of white marl layers in the NH-T section. The warm cycles 1, 4 and 6 at NH-T section probably correspond to three inferred warm periods reflected by high MS in the unit from 1.66-1.55 Ma of the XT section (Ao et al., 2010a), recorded by pollen data at the BS site (1.324-1.310 Ma; Yang et al., 2022) and as the upper lacustrine deposits (stage 3) of the XDK section (Li et al., 2010), respectively. Magnetite and hematite were identified as the dominant ferrimagnetic minerals in the E Nihewan Basin by Ao et al. (2009) and Liu et al. (2018). Olive green/pale-brown silts of the NH-T section have low MS values, whilst yellowish-brown silts/fine sands have typically high MS values. The higher MS values of the sand-dominated layers probably result from the redeposition of pedogenized loess and soils that were eroded and transported in the catchment during interglacials (Wang et al., 2006). Through the NH-T section, the χ_{FD} values are predominantly characterized by low and relatively constant values <2% which suggests the absence of paramagnetic grains influenced by Fe-reducing bacteria in soils (Dearing, 1999). Occasionally, there are moderate values between 2–11.4%, indicating soil formation and the incorporation of pedogenic ultrafine magnetite/maghemite grains into the NH-T sediments. The rarely higher χ_{FD} values >16% are observed in the inferred wetland and wetland-lake settings, indicating intensified soil formation and related warmer and wetter conditions when soil-derived particles were washed to wetlands and lakes. In contrast, the few high peaks observed in the inferred wetland-alluvial plain settings probably indicate soil erosion during colder climate conditions. For the corresponding drier intervals, Ao et al. (2009) reported an increased cooling coupled with an intensified aridification for the neighbouring XT section during 1.9-0.1 Ma, with low MS in the unit from 1.54-1.45 Ma as investigated by Ao et al. (2010b) which probably corresponds to the cooler cycles 2 and 3 at NH-T section. The pollen record from the Jinyuan Cave in NE China is characterized by a cooling and drying trend with large fluctuations from ca. 2.0-0.4 Ma and a transition from forest to forest-steppe vegetation between 1.7 and 1.5 Ma to the dominance of forest steppe until the Mid-Pleistocene Transition between 1.2 and 0.7 Ma (Shen et al., 2021). E Africa has experienced progressive aridification over the past few million years with precession-paced environmental shifts from closed forested ecosystems to open grassland ecosystems driven by moisture availability (Magill et al., 2013a; 2013b). Thus, the available evidence suggests that the high-latitude Nihewan Basin was characterized by significant environmental and long-term climatic fluctuations during the Early Pleistocene ca. 1.7–0.9 Ma. Therefore, early hominins apparently inhabited the environment of the Nihewan Basin from 1.66-0.78 Ma (Zhu et al., 2007), but probably not year-round or during cold periods (Dennell, 2013).

6 Conclusion

The exposed sediments of three sections T1-T3 (up to 50-m thick) in NE Nihewan Basin predominantly comprise varicoloured reworked silt-sized materials of aeolian origin, partially

interbedded with calcareous and fine-grained sand layers and minor contributions of clay-sized particles. Laminations of variable thickness, horizontal and ripple bedding, and bioturbation features have been recorded. Most of the sediments show unimodal GSDs with the occasional occurrence of bimodal and trimodal distributions. The sediments are poorly sorted, positive skewed, and characterized by mesokurtic and leptokurtic distributions. MS values of the sediment are generally low, and higher values were determined for the coarser-grained sediments. The recorded ostracod assemblages of the sediments are dominated by *Limnocythere* sp., *Ilyocypris* sp. and *Leucocythere* sp. The sediments also contain remains of gastropod shells. Prominent marker beds of white marl are apparently consistent and correlative throughout sections. Valves of *C. lacustris* were exclusively found in these white marl layers that support the correlation between the T1-T3 sections using the colour of the sediments and the presence of in situ-formed micritic carbonate in these beds. The correlation allowed to build a synthetic composite sedimentary section of 86.2-m thickness (NH-T) that was probably formed between ca. 1.7 and 0.9 Ma. Evidence from sedimentological and ostracod-assemblage data of the composite NH-T section suggests six remarkable depositional cycles of changing hydrodynamic conditions between dominantly a wetland with periods of lake and alluvial plain settings. The identified cycles evolve sequentially from 1) wetland and lake, 2) wetland, 3) wetland and alluvial plain, 4) wetland and lake, 5) wetland and alluvial plain, and ultimately, 6) wetland and lake conditions. This suggests that the high-latitude Nihewan Basin was characterized by significant environmental fluctuations during the time frame of the sediments studied here. The climate variability of Early Pleistocene is traced by three dominant fine-to coarse silt-sized components and ostracod-assemblage changes in the studied sediments. Three intervals of warmer and wetter climate and three intervals of colder and dryer climate are inferred. The inferred climate cycles likely represent climatic changes associated with astronomical (Milankovitch) forcing.

Nevertheless, an independent age model was not yet established for our sediment sections at Dachangliang, and further correlations with earlier studied sedimentary sequences with established magnetostratigraphy in the region will improve the chronological framework of inferred climate conditions. Furthermore, new analyses of sediments from additional sections within the E Nihewan Basin have good potential to better understand the cyclicity of environmental and landscape change in the basin during the Early Pleistocene.

Data availability statement

The original contributions presented in the study are included in the article/Supplementary Material, further inquiries can be directed to the corresponding authors.

References

Ao, H., An, Z., Dekkers, M. J., Wei, Q., Pei, S., Zhao, H., et al. (2012). High-resolution record of geomagnetic excursions in the Matuyama chron constrains the ages of the

Author contributions

Funding

Acknowledgments

Conflict of interest

The authors declare that the research was conducted in the absence of any commercial or financial relationships that could be construed as a potential conflict of interest.

Publisher's note

All claims expressed in this article are solely those of the authors and do not necessarily represent those of their affiliated organizations, or those of the publisher, the editors and the reviewers. Any product that may be evaluated in this article, or claim that may be made by its manufacturer, is not guaranteed or endorsed by the publisher.

Supplementary material

The Supplementary Material for this article can be found online at: https://www.frontiersin.org/articles/10.3389/feart.2024.1335360/full#supplementary-material

Feiliang and Lanpo paleolithic sites in the Nihewan Basin, north China. *Geochem. Geophys. Geosystems* 13, Q08017. doi:10.1029/2012GC004095

Ao, H., Dekkers, M. J., An, Z., Xiao, G., Li, Y., Zhao, H., et al. (2013b). Magnetostratigraphic evidence of a mid-Pliocene onset of the Nihewan Formation – implications for early fauna and hominid occupation in the Nihewan Basin, North China. *Quat. Sci. Rev.* 59, 30–42. doi:10.1016/j.quascirev.2012.10.025

Ao, H., Dekkers, M. J., Deng, C., and Zhu, R. (2009). Palaeoclimatic significance of the Xiantai fluvio-lacustrine sequence in the Nihewan Basin (North China), based on rock magnetic properties and clay mineralogy. *Geophys. J. Int.* 177, 913–924. doi:10.1111/j.1365-246X.2008.04082.x

Ao, H., Dekkers, M. J., Wei, Q., Qiang, X., and Xiao, G. (2013a). New evidence for early presence of hominids in North China. *Sci. Rep.* 3, 2403. doi:10.1038/srep02403

Ao, H., Deng, C., Dekkers, M. J., and Liu, Q. (2010a). Magnetic mineral dissolution in Pleistocene fluvio-lacustrine sediments, Nihewan Basin (north China). *Earth Planet. Sci. Lett.* 292, 191–200. doi:10.1016/j.epsl.2010.01.035

Ao, H., Deng, C., Dekkers, M. J., Liu, Q., Qin, L., Xiao, G., et al. (2010b). Astronomical dating of the Xiantai, Donggutuo and Maliang Paleolithic sites in the Nihewan Basin (north China) and implications for early human evolution in east Asia. *Palaeogeogr. Palaeoclimatol. Palaeoecol.* 297, 129–137. doi:10.1016/j.palaeo.2010.07.022

Barbour, G. B. (1924). Preliminary observations in the Kalgan area. *Bull. Geol. Soc. China* 3, 153–168. doi:10.1111/j.1755-6724.1924.mp3002009.x

Barbour, G. B., Licent, E., and Teilhard de Chardin, P. (1926). Geological study of the deposits of the Sangkanho basin. *Bull. Geol. Soc. China* 5, 263–278. doi:10.1111/j.1755-6724.1926.mp53-4005.x

Bi, Y., Pang, E., Sun, Y., Liu, Y., Bian, Q., Liu, S., et al. (2022). Magnetostratigraphy of the fluvio-lacustrine sequence of core DY-1 in the Datong Basin and its implications for the evolution of the Shanxi Rift System in northern China. *Palaeogeogr. Palaeoclimatol. Palaeoecol.* 599, 111063. doi:10.1016/j.palaeo.2022.111063

Blott, S. J., and Pye, K. (2001). GRADISTAT: a grain size distribution and statistics package for the analysis of unconsolidated sediments. *Earth Surf. Process. Landforms* 26, 1237–1248. doi:10.1002/esp.261

Chen, X. Q., Chi, Z. Q., Dong, S., Yan, Z., Yang, J., Shi, W., et al. (2015). Late Cenozoic sedimentation of Nihewan Basin, central north China and its tectonic significance. *J. Asian Earth Sci.* 114, 242–257. doi:10.1016/j.jseaes.2015.06.020

Chi, Z. Q., and Wei, Q. (2013). Study of "Nihewan Layer". *Stories Relics* 5, 3–10.

Dearing, J. (1999). "Magnetic susceptibility," in *Environmental magnetism, a practical guide. Technical guide No. 6*. Editors J. Walden, F. Oldfield, and J. Smith (London: Quaternary Research Association), 35–62.

Deng, C., Wei, Q., Zhu, R., Wang, H., Zhang, R., Ao, H., et al. (2006b). Magnetostratigraphic age of the Xiantai paleolithic site in the Nihewan Basin and implications for early human colonization of northeast Asia. *Earth Planet. Sci. Lett.* 244, 336–348. doi:10.1016/j.epsl.2006.02.001

Deng, C., Xie, F., Liu, C., Ao, H., Pan, Y., and Zhu, R. (2007). Magnetochronology of the Feiliang Paleolithic site in the Nihewan Basin and implications for early human adaptability to high northern latitudes in East Asia. *Geophys. Res. Lett.* 34, L14301. doi:10.1029/2007GL030335

Deng, C., Zhu, R., Zhang, R., Ao, H., and Pan, Y. (2008). Timing of the Nihewan formation and faunas. *Quat. Res.* 69, 77–90. doi:10.1016/j.yqres.2007.10.006

Deng, T., and Zheng, M. (2005). Limb bones of *Elasmotherium* (Rhinocerotidae, Perissodactyla) from Nihewan (Hebei, China). *Vertebr. Palasiat.* 43, 110–121.

Dennell, R. W. (2013). The Nihewan Basin of north China in the early Pleistocene: continuous and flourishing, or discontinuous, infrequent and ephemeral occupation? *Quat. Int.* 295, 223–236. doi:10.1016/j.quaint.2012.02.012

Ding, Z. L., Derbyshire, E., Yang, S. L., Yu, Z. W., Xiong, S. F., and Liu, T. S. (2002). Stacked 2.6-Ma grain size record from the Chinese loess based on five sections and correlation with the deep-sea δ^{18}O record. *Paleoceanography* 17, 725. doi:10.1029/2001PA000725

Domrös, M., and Peng, G. (1988). *The climate of China*. Berlin/Heidelberg: Springer. doi:10.1007/978-3-642-73333-8_9

Folk, R. L., and Ward, W. C. (1957). Brazos River bar: a study in the significance of grain size parameters. *J. Sediment. Petrol.* 27, 3–26. doi:10.1306/74d70646-2b21-11d7-8648000102c1865d

Hilgen, F. J., Lourens, L. J., Van Dam, J. A., Beu, A. G., Boyes, A. F., Cooper, R. A., et al. (2012). "The Neogene period," in *The geologic time scale* (Elsevier), 923–978. doi:10.1016/B978-0-444-59425-9.00029-9

Hu, X., Li, Y., and Yang, J. (2005). Quaternary paleolake development in the Fen river Basin, north China. *Geomorphology* 65, 1–13. doi:10.1016/j.geomorph.2004.06.008

Lebbink, M. J. I. (2010). *Aeolian late Eocene deposition in Xining, central China*. Dissertation/Master's thesis. Utrecht University.

Li, H., Yang, X., Heller, F., and Haitao, L. (2008). High resolution magnetostratigraphy and deposition cycles in the Nihewan Basin (North China) and their significance for stone artifact dating. *Quat. Res.* 69, 250–262. doi:10.1016/j.yqres.2007.11.002

Li, X., Huang, W., Wang, Y., and Ji, J. (2010). A study of the palaeoclimates and palaeoenvironments in the Nihewan Basin in the light of the lithofacies and the palaeontological remains of the Pleistocene mammals. *Chin. Sci. Bull.* 55, 297–306.

Li, Y. C., Xu, Q. H., and Yang, X. L. (1996). Pollen records of the Feiliang paleolithic site in Yangyuan, Hebei Province. *Geogr. Territ. Res.* 12, 55–59.

Li, Y. L., Yang, J., Xia, Z., and Mo, D. (1998). Tectonic geomorphology in the Shanxi Graben System, northern China. *Geomorphology* 23, 77–89. doi:10.1016/S0169-555X(97)00092-5

Lisiecki, L. E., and Raymo, M. E. (2005). A Pliocene-Pleistocene stack of 57 globally distributed benthic δ^{18}O records. *Paleoceanography* 20, PA1003. doi:10.1029/2004PA001071

Liu, P., Deng, C., Li, S., and Zhu, R. (2010). Magnetostratigraphic dating of the Huojiadi Paleolithic site in the Nihewan Basin, north China. *Palaeogeogr. Palaeoclimatol. Palaeoecol.* 298, 399–408. doi:10.1016/j.palaeo.2010.10.027

Liu, P., Yue, F., Liu, J., Qin, H., Li, S., Zhao, X., et al. (2018). Magnetostratigraphic dating of the Shixia red sediments and implications for formation of Nihewan paleo-lake, North China. *Quat. Sci. Rev.* 193, 118–128. doi:10.1016/j.quascirev.2018.06.013

Liu, T., An, Z., Yuan, B. N., and Han, J. (1985). The loess–paleosol sequence in China and climatic history. *Episodes* 8, 21–28. doi:10.18814/epiiugs/1985/v8i1/003

Magill, C. R., Ashley, G. M., and Freeman, K. H. (2013a). Ecosystem variability and early human habitats in eastern Africa. *Proc. Natl. Acad. Sci. U.S.A.* 110, 1167–1174. doi:10.1073/pnas.1206276110

Magill, C. R., Ashley, G. M., and Freeman, K. H. (2013b). Water, plants, and early human habitats in eastern Africa. *Proc. Natl. Acad. Sci. U.S.A.* 110, 1175–1180. doi:10.1073/pnas.1209405109

Meisch, C. (2000). *Freshwater Ostracoda of Western and Central Europe, Süßwasserfauna von Mitteleuropa 8/3*. Heidelberg: Spektrum Akad. Verlag, 522.

Meng, X., Liu, L., Wang, X. T., Balsam, W., Chen, J., and Ji, J. (2018). Mineralogical evidence of reduced East Asian summer monsoon rainfall on the Chinese loess plateau during the early Pleistocene interglacials. *Earth Planet. Sci. Lett* 486, 61–69. doi:10.1016/j.epsl.2017.12.048

Min, L. R., and Chi, Z. Q. (2003). *Quaternary geology of the Western Yangyuan Basin*. Beijing: Geological Publishing House.

Mischke, S., Herzschuh, U., Sun, Z., Qiao, Z., Sun, N., and Zander, A. M. (2006). Middle Pleistocene Ostracoda from a large freshwater lake in the presently dry Qaidam Basin (NW China). *J. Micropaleontol.* 25, 57–64. doi:10.1144/jm.25.1.57

Mu, H., Xu, Q., Zhang, S., Hun, L., Li, M., Li, Y., et al. (2015). Pollen-based quantitative reconstruction of the paleoclimate during the formation process of Houjiayao Relic site in Nihewan Basin of China. *Quat. Int.* 374, 76–84. doi:10.1016/j.quaint.2015.02.019

Munsell Soil Colour Chart (2009). *Munsell soil colour chart 2009 revised edition*. Baltimore, Maryland, USA: Macbeth Division of Kollmorgen Corporation.

Pang, Q., Zhai, D., Zhao, Z., and Zhang, Z. (2015). Late Cenozoic micropalaeontology in the Nihewan Basin and its implications for environmental evolution. *Acta Geol. Sin.* 89, 817–842.

Pei, S. W. (2002). The Paleolithic site at Dachangliang in Nihewan Basin, north China. *Acta Anthropol. Sin.* 21, 116–125.

Qiu, Z. X. (2000). Nihewan fauna and Q/N boundary in China. *Quat. Sci.* 20, 142–154.

Ruddiman, W. F., Raymo, M., Martinson, D. G., Clement, B. M., and Backman, J. (1989). Pleistocene evolution: northern hemisphere ice sheets and North Atlantic Ocean. *Paleoceanography* 4, 353–412. doi:10.1029/PA004i004p00353

Schick, K. D., Toth, N., Wei, Q., Clark, J. D., and Etler, D. (1991). Archaeological perspectives in the Nihewan Basin, China. *J. Hum. Evol.* 21, 13–26. doi:10.1016/0047-2484(91)90033-R

Shen, H., Zhao, K., Ge, J., Zhou, X., Song, Y., Liu, S., et al. (2021). Early and middle Pleistocene vegetation and its impact on faunal succession on the Liaodong Peninsula, Northeast China. *Quat. Int.* 591, 15–23. doi:10.1016/j.quaint.2020.11.034

Stuut, J.-B., Smalley, I., and O'Hara-Dhand, K. (2009). Aeolian dust in Europe: African sources and European deposits. *Quat. Int.* 198, 234–345. doi:10.1016/j.quaint.2008.10.007

Sun, M., Zhang, X., Tian, M., Liu, R., He, Z., Qi, L., et al. (2018). Loess deposits since Early Pleistocene in northeast China and implications for desert evolution in east China. *J. Asian Earth Sci.* 155, 164–173. doi:10.1016/j.jseaes.2017.09.013

Sun, Y., Lu, H., and An, Z. (2006b). Grain size of loess, palaeosol and Red Clay deposits on the Chinese Loess Plateau: significance for understanding pedogenic alteration and palaeomonsoon evolution. *Palaeogeogr. Palaeoclimatol. Palaeoecol.* 241, 129–138. doi:10.1016/j.palaeo.2006.06.018

Teilhard de Chardin, P., and Piveteau, J. (1930). Les mammifères fossiles de Nihowan (Chine). *Ann. Paleontol.* 19, 1–134. (hal-03266233).

Vandenberghe, J. (2013). Grain size of fine-grained windblown sediment: a powerful proxy for process identification. *Earth-Science Rev.* 121, 18–30. doi:10.1016/j.earscirev.2013.03.001

Walther, J. (1894). "Einleitung in die Geologie als historische Wissenschaft," in *Lithogenesis der Gegenwart* 3, 535–1055.

Wang, H., Deng, C., Zhu, R., Wei, Q., Hou, Y., and Boëda, E. (2005). Magnetostratigraphic dating of the Donggutuo and Maliang paleolithic sites in the Nihewan Basin, north China. *Quat. Res.* 64, 1–11. doi:10.1016/j.yqres.2005.04.001

Wang, H., Deng, C., Zhu, R., and Xie, F. (2006). Paleomagnetic dating of the Cenjiawan Paleolithic site in the Nihewan Basin, northern China. *Sci. China Ser. D.* 49, 295–303. doi:10.1007/s11430-006-02957

Wei, Q. (1983). A new *Megaloceros* from Nihowan beds. *Vertebr. Palasiat.* 21, 87–95.

Wei, Q. (1991). Geologic sequence of the archaeological sites in the Nihewan Basin, north China. *Contributions XIII INQUA* 1, 61–73.

Wei, Q. (2016). Textual research of Nihewan Basin. *Stories Relics* 2, 3–11.

Xia, Z. K. (1992). The study of the change of ancient lake shore in the Datong-Yangyan (Nihewan) Basin. *Geogr. Res.* 11, 52–59.

Xiao, J., Chang, Z., Fan, H., Zhou, L., Zhai, D., Wen, R., et al. (2012). The link between grain-size components and depositional processes in a modern clastic lake. *Sedimentology* 59, 1050–1062. doi:10.1111/j.1365-3091.2011.01294.x

Yang, J., Zhang, Z., Li, Y., Wang, F., Fan, B., She, Z., et al. (2022). Environment of the early Pleistocene Banshan Paleolithic site in the Nihewan Basin, north China. *Front. Earth Sci.* 10, 830798. doi:10.3389/feart.2022.830798

Yang, S., Deng, C., Zhu, R., and Petraglia, M. D. (2019a). The Paleolithic in the Nihewan Basin, China: evolutionary history of an early to late Pleistocene record in eastern Asia. *Evol. Anthropol.* 29, 125–142. doi:10.1002/evan.21813

Yang, X., Wang, X., Van Balen, R. T., Prins, M. A., Wang, S., van Buuren, U., et al. (2019b). Fluvial terrace formation and its impacts on early human settlement in the Hanzhong basin, Qinling Mountains, central China. *Glob. Planet. Change* 178, 1–14. doi:10.1016/j.gloplacha.2019.04.007

Young, C. C. (1950). "The Plio-Pleistocene boundary in China," in *Report on 18th International Geological Congress* (London: Wiley), 115–125.

Zhang, W., Mischke, S., Zhang, C., Gao, D., and Fan, R. (2013). Ostracod distribution and habitat relationships in the Kunlun Mountains, northern Tibetan Plateau. *Quat. Int.* 313–314, 38–46. doi:10.1016/j.quaint.2013.06.020

Zhu, R., Deng, C., and Pan, Y. (2007). Magnetochronology of the fluvio-lacustrine sequences in the Nihewan basin and its implications for early human colonization of Northeast Asia. *Quat. Sci.* 27, 922–944.

Zhu, R., Hoffman, K., Potts, R., Deng, C., Pan, Y., Guo, B., et al. (2001). Earliest presence of humans in northeast Asia. *Nature* 413, 413–417. doi:10.1038/35096551

Zhu, R., Potts, R., Xie, F., Hoffman, K., Deng, C., Shi, C., et al. (2004). New evidence on the earliest human presence at high northern latitudes in northeast Asia. *Nature* 431, 559–562. doi:10.1038/nature02829